JOURNAL OF GEOPHYSICAL RESEARCH, VOL. 99, NO. B5, PAGES 9615-9634, MAY 10, 1994

Western U.S. upper mantle structure

Eugene D. Humphreys and Kenneth G. Dueker

Department of Geological Sciences, University of Oregon, Eugene

Regional three-dimensional inversions of upper mantle P wave velocity structure are created from teleseismic P wave travel time residuals recorded by many of the high-density high-frequency regional arrays operated within the western United States. These inversions are adjusted to a global (International Seismic Centre) reference and merged to obtain an image of the upper mantle beneath western United States. The P wave velocities in the upper mantle are slow on average, and the structure is very heterogeneous. Where resolution is good, coherent upper mantle structures are imaged that extend as deep as ~200 km (the Juan de Fuca and Gorda slabs, which penetrate to greater depths, are exceptions) and deviate from the average velocity (at a given depth) by as much as ±4%. Lateral resolution of these structures usually is very good, although the magnitude of the actual seismic variations is probably greater than that imaged. The long wavelength part of the imaged mantle structure defines coherent elongate features with wavelengths of 200-500 km. Within ~250 km of the Pacific Coast, these structures have a wavelength of ~250 km and trend parallel to the surface physiography and young tectonic structures. Beneath the continental interior, where use is made of additional seismic studies to infer average structure in regions of poor teleseismic data coverage, structures have a wavelength of ~500 km and trend northeasterly. This northeast orientation is discordant with young tectonic structures but aligns with young volcanic activity.

Introduction

On average, western U.S. upper mantle seismic velocity is considerably slower than the upper mantle beneath the North American craton. *Cleary and Hales* [1966] were the first to note ~1 s differences in average P wave arrival time to stations on the North American craton compared to stations west of the Rocky Mountain Front. *Hales and Doyle* [1967], *Hales et al.* [1968] and *Hales* [1991] suggested that this large-scale dichotomy in arrival times arises from 3-6% variations in P wave velocity (V_P) within the upper few hundred kilometers of the mantle. Making use of a greater number of stations, the studies of *Romanowicz* [1979] and *Dziewonski and Anderson* [1983] served to accentuate and further define this large-scale seismic contrast. More recent waveform and tomographic studies have verified that P and S wave variations occur primarily in the upper mantle to depths of 200-400 km [*Burdick and Helmberger*, 1978; *Grand and Helmberger*, 1984; *Grand*, 1987]. *LeFevre and Helmberger* [1989] find that P wave velocities 50-200 km beneath the Canadian shield average ~8% faster than mantle of the same depth beneath the Gulf of California region [*Walck*, 1984]. In a global context, the average seismic velocity of the western U.S. upper mantle has been characterized as being typical of that beneath young oceanic crust [e.g., *Grand and Helmberger*, 1984; *Montagner and Tanimoto*, 1991]. In addition, it has been known for decades that variations in teleseismic P wave arrival time of ~1 s also occur between different regions within the western United States [*Cleary and Hales*, 1966], and highly variable upper mantle velocity structure has been imaged through waveform modeling of regional phases [*Archambeau et al.*, 1969; *Masse et al.*, 1972; *Gomberg et al.*, 1989] and through surface wave analysis [*Priestley and Brune*, 1982; *Taylor and Patton*, 1986; *Al-Khatib and Mitchell*, 1991]. Thus western U.S. upper mantle is both seismically slow on average and very heterogeneous.

The best resolved images of western U.S. upper mantle structure have been produced by inversions of teleseismic P wave arrival times recorded by high-density, high-frequency regional arrays distributed throughout the region. Typically, lateral variations in V_P of up to ~8% are imaged throughout the upper 200 km of the mantle beneath the western United States (southern California by *Raikes* [1980] and *Humphreys and Clayton* [1990]; northern and central California by *Zandt* [1981], *Benz et al.* [1992], and *Biasi and Humphreys* [1992]; Washington by *Michaelson and Weaver* [1986] and *Rasmussen and Humphreys* [1988]; southern Nevada by *Monfort and Evans* [1982] and *Biasi and Humphreys* [1992]; northern Nevada by *Iyer et al.* [1977]; eastern Snake River Plain and Yellowstone by *Evans* [1982] and *Iyer et al.* [1981]; eastern Great Basin by *Dueker and Humphreys* [1990]; and Rio Grande by *Parker et al.* [1984], *Spence and Gross* [1990], and *Davis et al.* [1993]). In this paper, we analyze teleseismic P wave residuals recorded by the 10 arrays shown in Figure 1 to develop a regional image of the upper mantle P wave velocity (V_P) structure for most of the western United States (Figure 2 shows locations of the geographic areas discussed). In order to merge the data from these arrays, we estimate and correct for the differences in average delay associated with each array.

The resulting upper mantle image shows coherent V_P structure that trends across the boundaries of individual arrays. The large magnitude (±4%) and great depth extent of the upper mantle velocity heterogeneity imaged beneath the western United States require large variations in the temperature and partial melt content of the upper mantle. Thus upper mantle V_P variations correspond to significant lateral variations in lithospheric strength, density and composition. As a result, the imaged upper mantle velocity structure is thought to control the ongoing volcanic and tectonic activity.

Paper number 93JB01724.
0148-0227/94/93JB-01724$05.00

Method

Teleseismic P Wave Data

Our data are ~44,000 teleseismic P and *PKIKP* phases recorded on ~1000 high-frequency vertical-component seismometers that contribute to the following permanent and temporary arrays (see Table 1 and Figure 1): Washington Regional Seismic Network (Washington and northern Oregon) augmented with data derived from a temporary array deployed in western Oregon [*Iyer and Rite*, 1981] and a temporary line array deployed across southwestern Oregon [*Harris et al.*, 1991]; Utah array (eastern Great Basin) augmented with data from two line arrays across the eastern Snake River Plain [*Evans*, 1982] and data

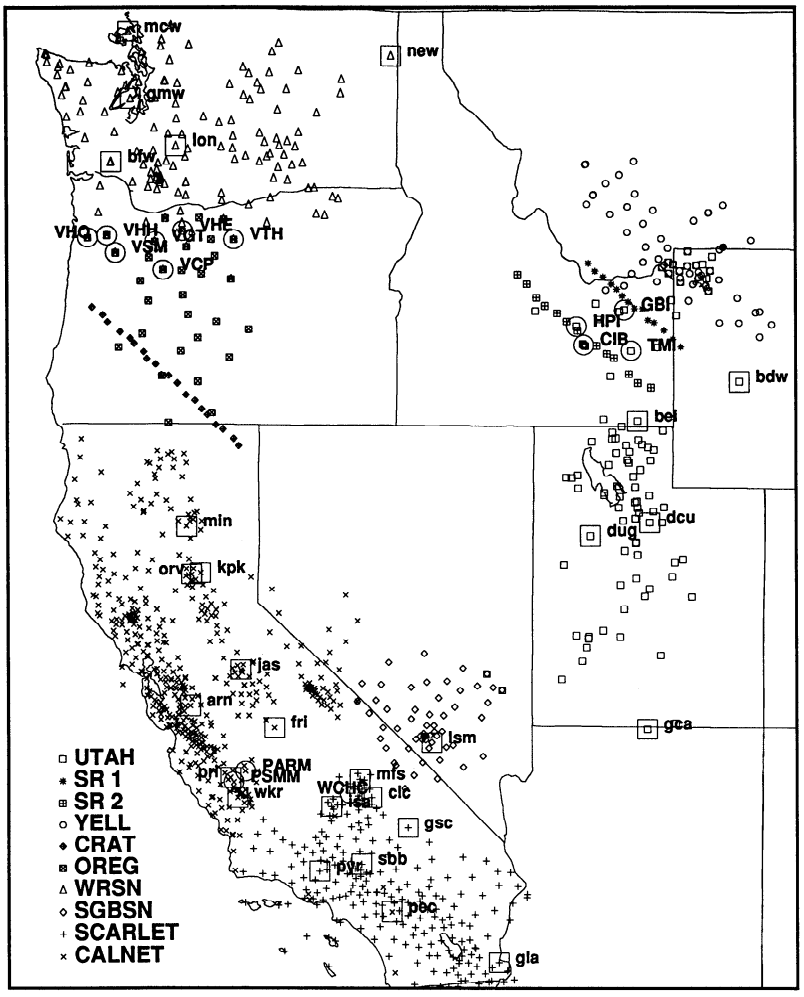

Fig. 1. Station map. Array associations for individual stations are given by symbol types shown in legend. Array abbreviations are Utah array (UTAH); Snake River 1 experiment (SR1); Snake River 2 experiment (SR2); Yellowstone array (YELL); Crater Lake experiment array (CRAT); a temporary Oregon array (OREG); Washington Regional Seismic Network (WRSN); southern Great Basin seismic network (SGBSN); southern California array (SCARLET); and northern and central California array (CALNET). Squares with adjacent station names identify stations with estimated absolute residuals from *Dziewonski and Anderson* [1983] (see Table 3). Circles with adjacent station names represent stations that are shared by more than one array (see Table 2).

from the Yellowstone region [*Iyer et al.*, 1981]; southern Great Basin seismic network (southern Nevada); southern California array (southern California); and California network (central and northern California). *P* wave arrival times have been hand picked (either by us or by those who originally collected the data) with an estimated error of less than 0.1 s. To minimize the large timing errors associated with cycle mispicks, all residuals have been inspected for consistency both on an event by event and on a station by station basis and obvious outliers have been removed. All travel times are reduced to absolute residuals with use of the radial Earth model PREM [*Dziewonski and Anderson*, 1981]. Relative residuals are then created by subtracting the average absolute residual for each event. Removal of this event mean (i.e., demeaning) is necessary to minimize potential errors arising from uncertainties in event origin parameters, lower mantle structure and the reference Earth model inaccuracies.

Inversion Method

Inversion algorithm. The model consists of constant slowness 20×20×20 km cubes, of which ~100,000 are hit well enough to contribute significantly to our inversion. We seek the set of slowness values for these cubes that "best" account for the data in a least squares sense. Rays are traced through this model using an assumed one-dimensional velocity structure. Minor deviations from the assumed structure, either in depth or laterally, have negligible effect on the ray location for teleseismic rays in the upper mantle beneath the recording sites [*Humphreys and Clayton*, 1990; *Rasmussen and Humphreys*, 1988]. Matrix inversion of the least squares normal equations is accomplished using the LSQR algorithm [*Paige and Sanders*, 1982a, b; *Nolet*, 1985]. A smoothness constraint is imposed on the inversion by pre-conditioning the system of equations with an a priori model covariance matrix [*Tarantola and Vallete*, 1982; *Meyerholtz et al.*, 1989]. We choose a 50% correlation between each moded parameter and its eight nearest neighbors in a horizontal layer. No a priori vertical smoothing is imposed because of the strong intrinsic model covariance in this direction resulting from the dominately vertical orientation of teleseismic rays.

Crustal model parameters are not smoothed in our inversion because significant variations in crustal structure are known to occur with dimensions similar to our block size. However, the absence of smoothing permits crustal model parameters to attain

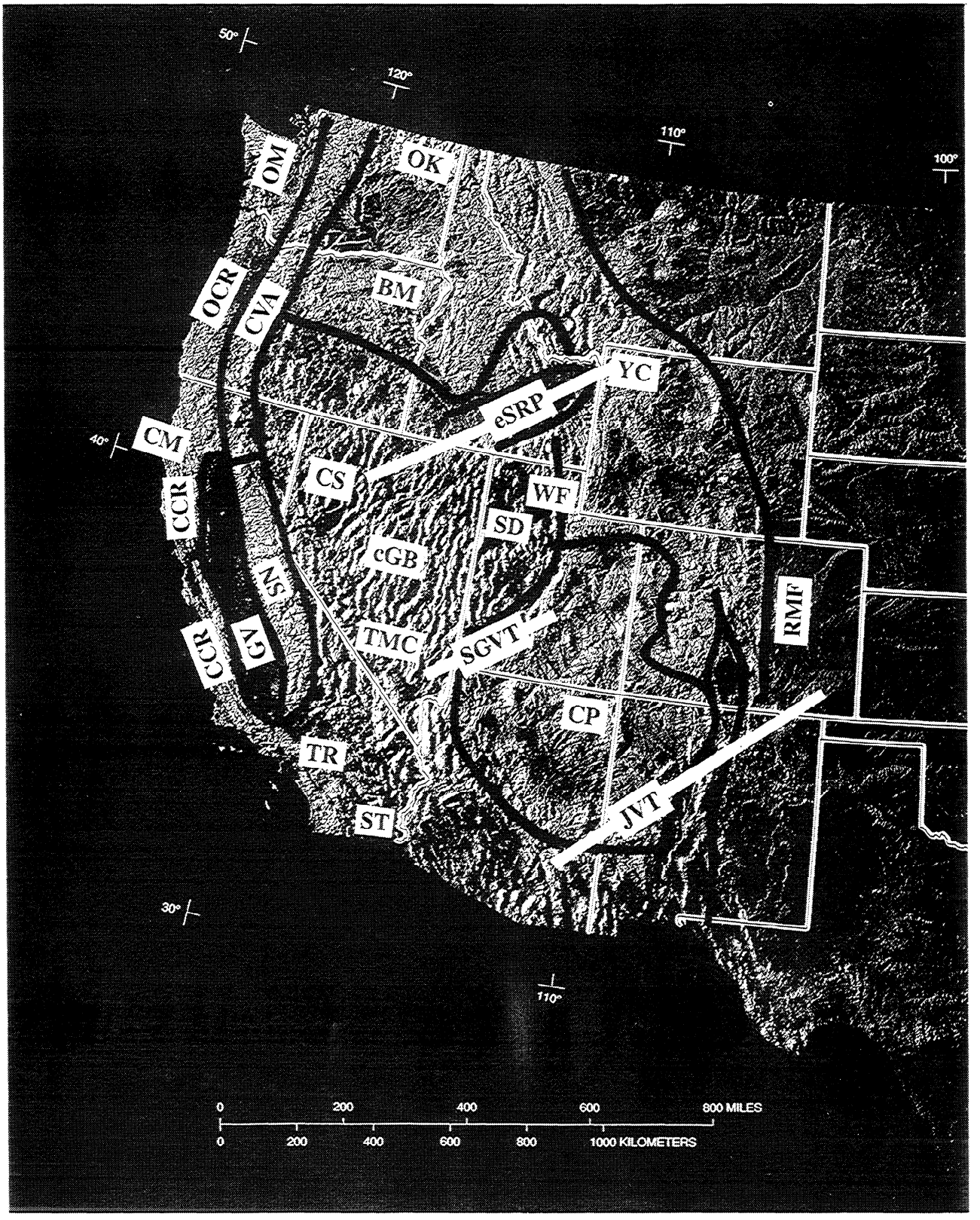

Fig. 2. Western U.S. topography and geographical features. Labeled features are BM, Blue Mountains; CCR, California Coast Ranges; cGB, central Great Basin; CM, Cape Mendocino; CP, Colorado Plateau; CS, Carson Sink; CVA, Cascade volcanic arc; eSRP, eastern Snake River Plains; GV, Great Valley; JVT, Jemez volcanic trend; OCR, Oregon Coast Ranges; OK, Okanogan Highlands; OM, Olympic Mountains; RMF, Rocky Mountain Front; SGVT, St. George Volcanic Trend; SD, Sevier Depression; SN, Sierra Nevada; ST, Salton Trough; TMC, Timber Mountain Caldera; TR, Transverse Ranges; WF, Wasatch Front; YC, Yellowstone Caldera.

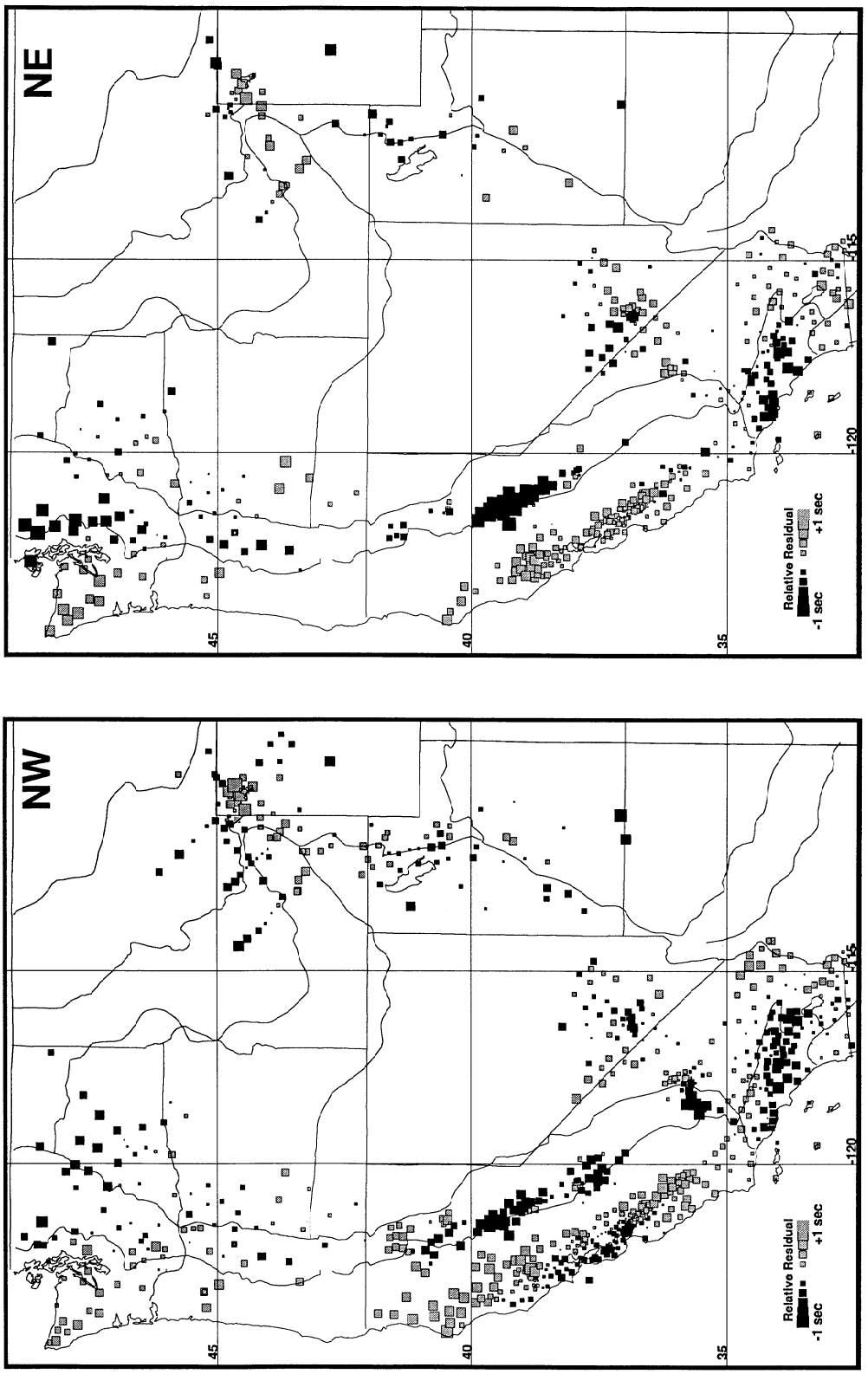

Fig. 3. *P* wave station residuals for phases from the indicated azimuthal quadrants. Solid and shaded symbols denote early and late arrivals, respectively, with symbol size proportional to absolute value of delay. Symbol magnitudes are clipped at ±1 s to accentuate typical variations, but some residuals deviate from average by 1.5 s. The spatial shift of residual patterns between opposing backazimuths is roughly equal to the depth of a causative velocity anomaly. For example, the systematic shift of the residual patterns associated with the eastern Snake River Plain, the Transverse Ranges, and the Juan de Fuca slab require an upper mantle origin. For reference, province boundaries are shown.

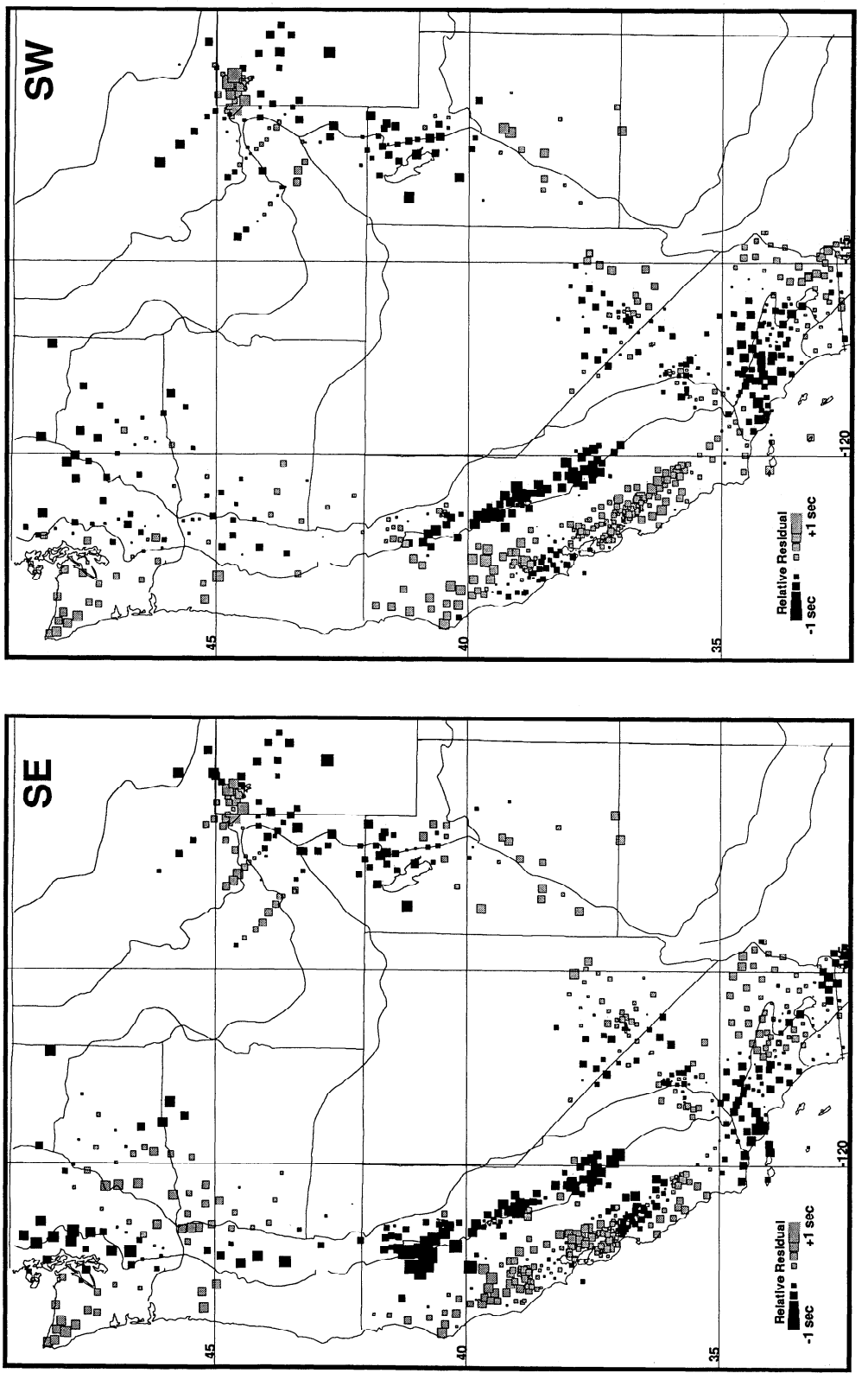

Fig. 3. (continued)

TABLE 1. Data and Inversion Parameters

	Pacific Northwest				California-Nevada				Eastern Great Basin					Net
	Wash-ington	Oregon	Crater Lake	Net	Northern California	Southern California	Southern Nevada	Net	Utah	Yellow-stone	SR1	SR2	Net	
Total number of station	120	31	20	171	368	216	56	640	80	52	12	11	155	966
Total number of rays	3724	1098	562	5384	17,319	12,896	3324	33,539	2393	1625	825	428	5271	44,194
Avgerage rays per station	31	35	28	-	51	55	60	-	36	34	56	28	-	-
Total number of events	71	90	41	-	109	204	78	-	71	138	73	43	-	-
Avgerage stations per event	54	13	14	-	162	67	44	-	36	13	12	11	-	-
Data RMS (s)	0.45	0.33	0.31	0.42	0.40	0.32	0.26	0.36	0.48	0.45	0.34	0.32	0.44	0.39
Residual RMS (s)	0.18	0.11	0.14	0.16	0.21	0.18	0.16	0.19	0.23	0.18	0.12	0.12	0.24	0.19
Avgerage event static (s)	.05±.07	-.09±.08	-.05±.06	-	.00±.04	-.05±.06	.06±.06	-	.06±.06	-.05±.20	.03±.07	.08±.09	-	-
Percent RMS reduction	60	67	55	62	48	44	38	47	52	60	65	62	45	51

Each of the 10 arrays used in this study are shown grouped into their respective array clusters. An inversion was performed for each cluster, and avgerage event static is with respect to the inversion for the cluster to which the array belongs. The range given for the average event static values represents one standard deviation. Percent RMS reduction refers to the root-mean-square reduction in delay values resulting from inversion (associated variance reductions range from 73 to 89%).

unreasonably large values. This problem is addressed by constraining the root mean square (RMS) value of the crustal model parameters to equal that of the mantle model parameters, which is accomplished by rescaling the columns of the data kernel matrix that are associated with the crustal parameters.

Station statics. Delays caused by crustal structure can be significant. However, in many portions of the western United States, independent seismic data exist that permit good estimates of crustal correction terms. Hence we need to judge how well these corrections are estimated and to understand the influence on the inversion of crustal correction terms that are incorrect or absent.

The simplest indication that crustal structure is not the dominant source of teleseismic delay is provided by the residual patterns seen from opposing backazimuths (Figure 3). These show coherent patterns of delay that shift by distances which are too great to have a crustal origin. Further qualitative support is lent by the fact that most of the observed teleseismic delay patterns are opposite in sign to what would be expected from known crustal structure. For example, early arrivals are observed to the Cascades and Sierra Nevada (Figure 4), where thick crust has been inferred [*Mooney and Weaver*, 1989].

A more quantitative argument is provided by comparing the RMS value of the observed teleseismic delays with the estimated RMS value of crustal delays. Histograms of North American crustal velocity and thickness [*Mooney and Braile*, 1989] create variations in teleseismic delays with RMS values of about 0.2 s and 0.25 s, respectively (compared with an observed data RMS of ~0.4 s for teleseismic arrivals). However, delays caused by structures of dimension shorter than our model parameterization are uncorrelated when projected to upper mantle depths and therefore do not contribute to the image of the upper mantle structure; as incoherent signal, these delays are part of the unmodeled residuals in our inversion. Of more concern is crustal structure that is coherent on dimensions roughly equal to or greater than our model parameterization. The magnitude of crustal structure at these wavelengths can be estimated directly with the use of the station time terms calculated in P_n studies. This approach is especially useful because the rays associated with these terms traverse the crust from the Moho to the actual stations used in our teleseismic analysis, thereby providing a good estimate of the average crustal delay in the vicinity of these stations. This averaging occurs with a horizontal length scale of about 30 km at the Moho [e.g., *Hearn and Clayton*, 1986], which is similar to the 20-km block size used in of our inversion. P_n crustal studies have occurred using the arrays in southern California, central California, and Washington by *Hearn and Clayton* [1986], *Oppenheimer and Eaton* [1984], and *Zervas and Crossen* [1986], respectively. The RMS of teleseismic station delays estimated with P_n station time terms is ~0.1 s. This signal is relatively small compared to the teleseismic residuals, suggesting that delays caused by crustal structure does not strongly influence the inversion of the upper mantle. Where P_n studies have been done, the station time terms are used to correct for crustal structural variations, thereby directly accounting for much of the signal produced by the crust.

Where P_n studies are not available, resolution usually is inadequate to image delays created in the crust solely as crustal structure (unless the station spacing is less than about 15 km). The severity of the problem of not having crustal correction terms available has been examined for two regions where high quality data are available on crustal structure (southern California [*Humphreys and Clayton*, 1990] and Washington [*Rasmussen and Humphreys*, 1988]). Comparisons made between inversions that used corrected data and inversions that used uncorrected data indicate that omission of crustal corrections results in different images of the crust and upper mantle to depths roughly equal to the minimum horizontal dimension of

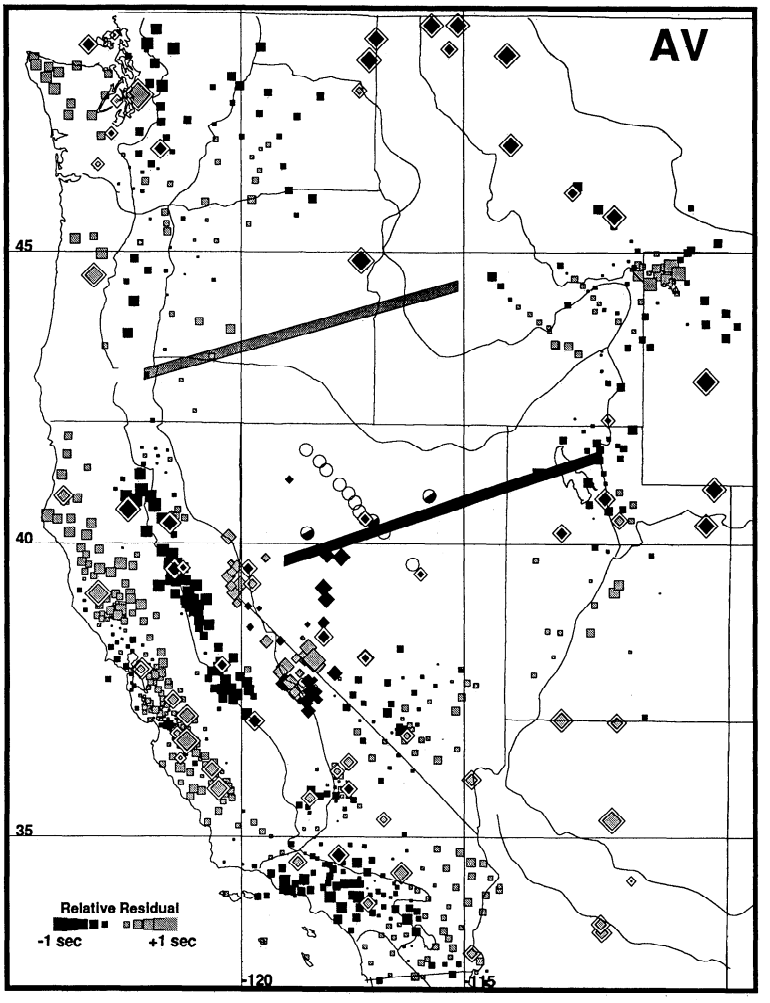

Fig. 4. Average P wave station residuals and additional seismic information on upper mantle structure. Solid and shaded symbols denote early and late arrivals, respectively, with symbol size proportional to absolute value of delay. Symbol magnitudes are clipped at ±1 s to accentuate typical variations, but some residuals deviate from average by 1.5 s. Squares represent the average delay to stations used in this study, where the average is performed over the four delta-azimuth subsets shown in Figure 3 plus a bin for the core phases. For reference, province boundaries are also shown. To extend the seismic coverage into the central Great Basin and other areas of poor seismic coverage, we include (1) average ISC residuals from *Dziewonski and Anderson* [1983] with the 0.56 s western U.S. average removed (diamond symbols with a white border), (2) average station residuals from the northern Nevada array [*Dueker and Humphreys*, 1990] (unbordered diamond symbols), (3) stations with ~1 s relative delay in arrivals from northwest backazimuths compared to those from the southeast [*Koizumi et al.*, 1973] (half-solid circles in northern Nevada), (4) stations from a temporary experiment whose station residuals have been interpreted as indicating a ~200-km-deep high-velocity body beneath the southeast end of the NW-SE trending line array [*Iyer et al.*, 1977, also personal communication, 1991] (open circles in northern Nevada), and (5) surface wave studies, with upper mantle velocities ~8% faster in northern Nevada than in southeastern Oregon [*Priestley and Brune*, 1982] (solid and shaded bars in the northern Great Basin).

the crustal structure. The degree to which the images are different usually is not pronounced, and large-scale aspects of the imaged upper mantle structure are not effected. The largest crustal correction terms occur for stations located on the deep sedimentary basins. Fortunately, the available P_n studies cited above include the deep sedimentary basins, and hence these delays are well estimated.

Of the regions where P_n station time terms are not available, the crustal feature of most concern is the Yellowstone caldera. Crustal delays in the Yellowstone region are estimated to be 0.2-0.4 s in the caldera and possibly up to 0.5-0.75 s for those rays that pass through the caldera magma chamber [*Smith et al.*, 1983]. Insufficient independent information exists to estimate individual station statics there, and crustal corrections are not applied. However, the dense set of stations in this region permits isolation of large-scale crustal effects (i.e., at the scale of our block size) from mantle effects. The seismic velocity of the crustal blocks in the caldera region of our inversion account for 0.3 s of delay.

Thus we conclude that most crustal delays are well accounted for, and residual effects resulting from inaccurate or incomplete crustal information do not present a serious problem to the imaging of the upper mantle.

Event statics. Demeaning of the data to create relative residuals involves a time shifting of the data so that the residuals for each event has zero mean. However, because each event samples the upper mantle differently, the mean delay for each event should differ somewhat from zero. (For example, imagine a situation where actual V_P structure is slow beneath the west half of an array and fast beneath the east half. If only stations in the west half of the array happened to record an event, the average delay would be greater than what the array normally records. When these hypothetical data are demeaned, an adjustment is needed to correct for this effect.) For each event, the

time adjustment that minimizes the differences between the event's relative residuals and the values predicted by the inversion is calculated and applied. This time adjustment is the best estimate of the desired correction, and it is termed the event static. Calculation and application of event statics are done with the use of constraint equations. Event statics are calculated simultaneously with the estimation of slowness values during inversion.

Event statics are small for most events, usually less than 0.1 s. However, if a geographically limited set of stations records an event, larger event statics sometimes result. The most extreme example of such time-biased data is those from the Yellowstone region, where a frequent relocation of 8-20 seismometers resulted in data with event statics as large as 1 s. The large standard deviation in the event statics for the Yellowstone array (Table 1) reflects these relatively large statics.

Array statics. With the use of information shared between adjacent arrays, the 10 individual arrays shown in Figure 1 are combined into three array clusters: the Pacific Northwest, eastern Great Basin, and the California-Nevada clusters. Thus we need to estimate the relative time shifts that need to be applied in order to construct array clusters. Two means are used to do this:

1. A comparison is made of residuals recorded by any station shared by adjoining arrays or by two stations from different arrays that are geographically very close (Figure 1 shows these stations with large circles). An arrival from a particular event to a particular station that is recorded by two arrays should have the same arrival time; however, because each data set has been demeaned with respect to its own array, the observed delay will differ by an amount equal to the difference between the average arrival times of the two arrays. Because the data sets used in our study have been picked by different researchers at different times, few events are actually shared between arrays. However, data to shared (or nearby) seismometers associated with rays of similar geometry are abundant. The time shift that minimizes the difference between these observed data is calculated and used to estimate the relative time shifts between the Oregon and Washington arrays and the southern California and northern California arrays (Table 2). These time shifts are imposed during inversion. The largest shift is 0.18 s between the Washington and Oregon arrays (with Oregon arrivals being later).

2. Event statics are used to estimate the relative time shift between arrays in cases where the arrays are close enough that ray paths share significant volumes of upper mantle. The ability to estimate the array static between arrays with the use of event statics depends on the connectivity between the two ray sets through shared model parameters. Quantitative assessment of this connectivity requires assembly of the resolution matrix, which is impractical for the dimensions of our inversion. A qualitative assessment of array connectivity can be made by noting the station overlap between different arrays (Figure 1).

Between the Oregon and Washington arrays and between the northern and southern California arrays the relative time shifts can be estimated either with the use of shared stations or with event statics. Time shifts estimated with event statics are compared to those calculated through the use of common stations (Tables 3 and 4), and the two approaches prove to be different by less than 0.05 s.

Joining array clusters. To find a common time base among the three array clusters, we make use of the 26 stations that have recorded data both as members of western U.S. arrays and as part of the global International Seismological Centre (ISC) array (see Figure 1 and Table 3). Long-period and low-gain stations, which are known to provide a systematic bias in ISC-reported arrival times [*Grand*, 1990], are excluded. For our data, we consider a well-hit station to have at least four rays in at least three of four azimuthal quadrants, whereas we consider a well-hit ISC station to have at least 99 recordings distributed within six of the 18 azimuthal bins used by *Dziewonski and Anderson* [1983]. From these stations, an average residual is calculated for each data set and the two times are subtracted to yield the estimated time shift between our (zero mean) observed data and the (absolute) ISC residuals (Table 4). No differences greater than 0.1 s exist among the average travel time residuals for the different western U.S. array clusters. After applying the small relative time adjustments estimated for each of the three array clusters, our western U.S. station residuals are found to average 0.56 s late with respect to PREM, with a standard deviation of 0.24 s. The average delay indicates a slow average seismic velocity of western U.S. upper mantle, and the standard deviation indicates significant heterogeneity there. Figure 5 is a histogram of all the relative residuals used in our study.

TABLE 2. Common Array Station Comparison

Stations		Proximity, km	Difference ± s.d., s
Oregon	Washington		
vhov	VHO	0	-0.26
vhhv	VHH	1.4	-0.09
vgtv	VGT	0	-0.25
vcpv	VCP	0	-0.24
vsmv	VSM	0	-0.11
vthv	VTH	0	-0.07
vhev	VHE	0.9	-0.26
			-0.18±0.08

Stations		Proximity, km	Difference ± s.d., s
Utah	SR2		
TMI	SK4B	7.8	0.0
GBI	SR7B	16.2	0.07
HPI	SK8	8.3	0.0
CIB	SK7	2.5	0.05
			0.03±0.03

Stations		Proximity, km	Difference ± s.d., s
Southern California	Northern California		
PARM	PARM5	0	-0.06
PSMM	PSMM5	0	-0.01
WCHC	WCHC5	0	-0.16
			-0.08±0.07

Comparison of the difference in the average residual for those stations that reported data to two arrays or for two different stations that are geographically close. By averaging these differences, the average time shift between two arrays is estimated. Note that only the shift between the Oregon and Washington arrays differs significantly from zero, with the Oregon array being 0.18 s slow with respect to the Washington array.

RESOLUTION

Resolution depends on the distribution of rays that sample a region, including both the number of rays and their range in incidence angle and azimuth. Of the set of models that best account for the data in a least squares sense, our inverse is a model of minimum energy. This results in a relatively low amplitude, spatially distributed reconstruction. Because teleseismic rays are strongly biased toward a vertical orientation (most rays have an angle of incidence of about 35° from vertical), resolution kernels are elongate in this direction, and the imaged structure is streaked vertically. For this reason, teleseismic rays do not provide good resolution of features that are laterally broad compared to their thickness, even if the region is well sampled. An extreme example of poor resolution resulting

TABLE 3. Comparison of Station Residuals: ISC Versus Arrays

Array	Station	ISC, s	Us, s	Us-ISC ±s.e.
Washington	new	-0.37	-0.57	0.20
	mcw	0.56	-0.19	0.75
	lon	0.16	-0.23	0.39
	gmw	0.63	0.02	0.61
				0.49±0.12
Utah	gca	0.96	0.14	0.82
	dug	0.22	-0.17	0.39
	dcu	0.84	0.10	0.75
	bei	0.44	0.08	0.37
	bdw	-0.56	-0.97	0.41
				0.55±0.10
Northern California	arn	0.93	0.29	0.64
	fri	0.12	-0.54	0.66
	jas	0.30	-0.20	0.50
	kpk	0.44	-0.17	0.61
	min	-0.07	-0.56	0.49
	orv	0.05	-0.39	0.44
	fri	1.08	0.47	0.61
	wkr	1.35	0.17	1.18
	mfs	0.71	0.03	0.68
				0.64±0.07
Southern California	sbb	0.03	-0.04	0.07
	pyr	0.89	0.06	0.84
	pec	0.83	-0.09	0.92
	isa	0.86	-0.04	0.90
	gsc	0.72	0.17	0.56
	gla	0.87	0.23	0.64
	clc	0.30	-0.01	0.31
				0.60±0.14
Southern Nevada	lsm	0.73	0.21	0.52

Comparison between average station residuals calculated from our data and average absolute station residuals from International Seismological Centre (ISC) data [*Dziewonski and Anderson*, 1983]. The difference between these residuals represents the time shift needed to bring our demeaned residuals into coincidence with the ISC station residuals (because all residuals recorded by an array are demeaned together, the time shift for all stations within an array are the same). The best estimate of this time shift is determined by averaging all available differences from each array. This average is shown as the last entry for each array. The standard error associated with each average represents the uncertainty in this estimate. After subtracting the average western U.S. ISC residual of 0.56 s, the relative array statics range between -0.07 and 0.08 s; that is, average array delays are not resolvably different from one another or from the average western U.S. delay.

from a broad structure is that of an anomalous horizontal layer extending completely across the model; in this case there is no resolution on the depth of this feature. This can be understood by recognizing that all rays from a given teleseismic event would be equally delayed regardless of the depth of the anomalous layer.

Regions of thorough ray sampling, and hence good depth resolution, include much of southern Washington, south central California, the eastern Snake River Plain, and the California Coast Ranges. Where sampling is inadequate to provide good depth constraint, a distinction cannot be made between a thick, low-amplitude structure and one that is of greater seismic contrast and vertically more compact. Our inverse is underconstrained in many regions, and in these regions, vertical resolution is poor and imaged amplitudes will be low. However, even in these regions, teleseismic rays allow for accurate resolution of lateral variations in structure. Hence the imaged lateral variations in upper mantle structure are authentic features.

A qualitative map of resolution that takes into account both the number and the geometrical diversity of the rays hitting a block is shown in Figure 6. Inversions of synthetic data created by test structures indicate that regions having a hit quality greater than 0.6 have good lateral resolution and usually have depth resolution of about ±50 km for laterally confined features. Regions of poor hit quality have essentially no depth resolution and resolve only lateral variations in upper mantle structure.

A test that indicates resolution of local structure is shown in Figures 7 and 8. The input structure consists of 60 km × 60 km high- and low-velocity vertical "posts" in the depth interval 40-200 km. The ray set is traced through this structure, and synthetic delays are calculated. Three sets of random noise are then added to these delays, each with an RMS value of 10% that of the synthetic delays. The three sets include noise added to each of the individual residuals, to all residuals from each event, and to all residuals recorded by each station. These synthetic data are then inverted in the same manner as real data. Upon inversion, lateral resolution of the posts is seen to be excellent (Figure 7). In cross section (Figure 8), vertical resolution of the base of the posts is seen to vary greatly. Generally, the anomalous velocities associated with the posts are streaked down 20-100 km beneath the actual base of the posts. In most cases, the tops of the posts are well resolved. Reconstructed amplitudes of over 75% are attained in the well resolved regions, whereas amplitudes in poorly hit regions are low. These test inversions use synthetic data that have been demeaned on an array-by-array basis (same as the actual data). During inversion, array statics are estimated, and for arrays where event statics are used to estimate relative array time shifts, calculated event statics recover ~70% of the proper value in average. The southern Nevada array is an exception, where the calculated event static is only 30% of its true value. Test inversions using different test structures produce very similar estimates of the array static values.

WESTERN U.S. RESIDUALS

Average station residuals are shown in Figure 4. The delays to stations within each cluster have been adjusted so as to minimize misfit with the ISC-reported residuals (Table 3), and 0.56 s has been subtracted from all values in order to emphasize the variations about the western U.S. mean. Each value shown in Figure 4 is a weighted average of the four azimuth averages shown in Figure 3 plus core phases (where these are available) and represents an average of the velocity structure beneath that station. The residuals have an average RMS value of 0.4 s and show coherent spatial variations of up to 2 s. Figure 4 indicates the highly heterogeneous nature of the western U.S. velocity structure. As discussed in the station statics section above, these residuals are created primarily by upper mantle seismic structure, and not by crustal seismic structure.

To produce a 1 s residual for a teleseismic event requires a ~6% V_P anomaly distributed over 100 km in depth (and a 2 s residual requires a ~12% V_P anomaly over 100 km, or a ~6% V_P anomaly over 200 km, etc.). The delay patterns in Figure 4 define coherent regions: late arrivals occur along the California Coast Ranges; early arrivals occur beneath the Cascades; early arrivals occur in the vicinity of the Transverse Ranges; late arrivals occur along the eastern Snake River Plain; and late arrivals are associated with the St. George Volcanic Lineament and its continuation across southern Nevada. The compilation of these data onto one map with a common time base shows a continuity in residual patterns across the array boundaries,

TABLE 4. Summary of Delays Relating Local Arrays

	Pacific Northwest			California-Nevada			Eastern Great Basin			
	Wash-ington	Oregon	Crater Lake	Northern California	Southern California	Southern Nevada	Utah	Yellow-stone	SR1	SR2
Common station	-0.06*	0.12*	-	-0.04*	0.04*	-	-0.06	-	-	-0.04
Event static	-0.04	0.10	0.06*	-0.01	0.00	0.05*	-0.04*	0.07*	-0.01*	-0.06*
ISC	-0.07	-	-	0.08	0.08	-	0.01	-	-	-

Delays are in seconds. Common station and event static delays compare array delays within an array cluster, and ISC delays compare array clusters. Positive values represent relatively late arrivals. The most important point is that all relative differences are small. Common station comparison values are from Table 2, though an arbitrary constant is added to the set of delays from each cluster shown in Table 2, so that the relative delays can be compared to the event statics (the addition of a constant is justified because the values shown in Table 2 only represent relative differences). Event statics are calculated during inversion (and average zero when weighted by the number of rays recorded by each array); the values shown here are those determined with no prior time adjustments applied to the array data and thus represent the estimated full difference between the two arrays. ISC-based comparisons are from Table 3, where the average western U.S. delay of 0.56 s has been subtracted. These are the values used to adjust each cluster with respect to one another (and with respect to global average).

*Delay values actually applied to the data in order to create a set of residuals within each cluster of arrays that is on a common time base. Other values are shown for comparative purposes.

demonstrating that no gross array static problems exist. For example, the Yellowstone and eastern Snake River Plain data define a continuous region of late arrivals extending southwest from Yellowstone and widening from 50 km at Yellowstone to ~100 km at a distance of 200 km southwest of Yellowstone. Also, the southwest trending region of late arrivals associated with the St. George volcanic field extends across southern Nevada into southern California.

Figure 3 shows maps of average residual to each station for each of four delta-azimuth bins. Most stations exhibit large azimuthal variations in residual value (up to 1.5 s). The spatial shift in the residual patterns with respect to event backazimuth provides a direct indication of the depth of the causative velocity structures. For example, considering that the range in upper mantle angle of incidence for direct P is 30-45° (measured from vertical), a structure buried at 100 km depth is associated with a residual pattern shift of ~125 km between opposing backazimuths. A good example of spatial shift in residual pattern is observed along the eastern Snake River Plain, where late arrivals associated with an underlying low velocity feature shift by ~100 km between arrivals from northwest and southeast back-azimuths. Other examples are associated with the early arrivals to stations near the Transverse Ranges and the Cascade volcanic arc. Such well-defined spatial shifts in the residual patterns provide convincing evidence that compact velocity variations exist in the upper few hundred kilometers of the mantle. Furthermore, the fact that these shifting delay patterns are roughly constant in magnitude from different backazimuths suggests that upper mantle anisotropy is not strongly influencing the observed P delays.

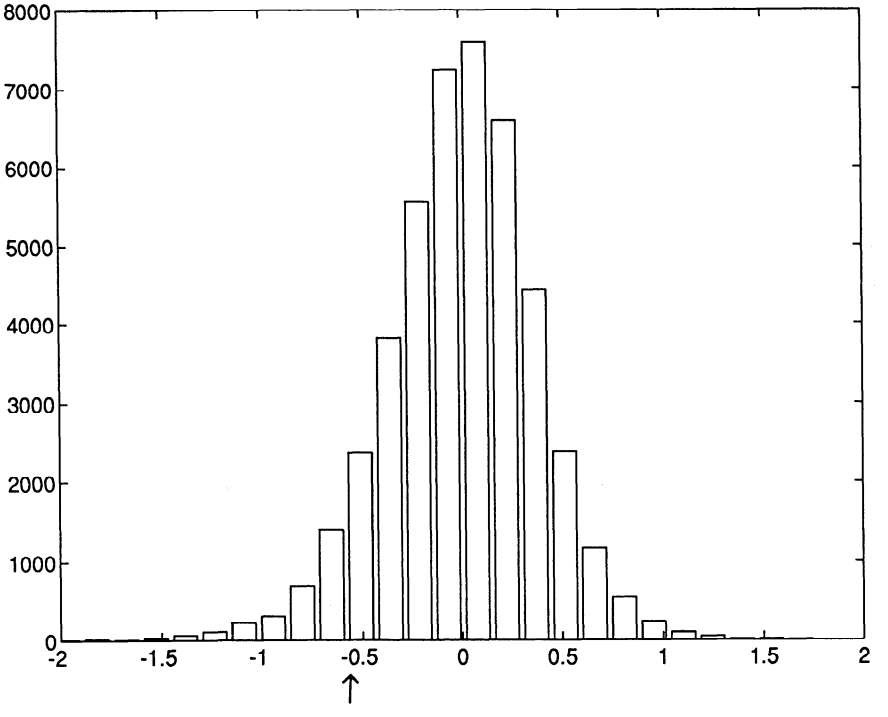

Fig. 5. Histogram of 44,000 P wave residuals used in this study. Arrow shows the average arrival time estimated for the whole Earth [*Dziewonski and Anderson*, 1981]. Although most of the arrivals are late with respect to global average, arrivals about 1 s early are recorded at some stations.

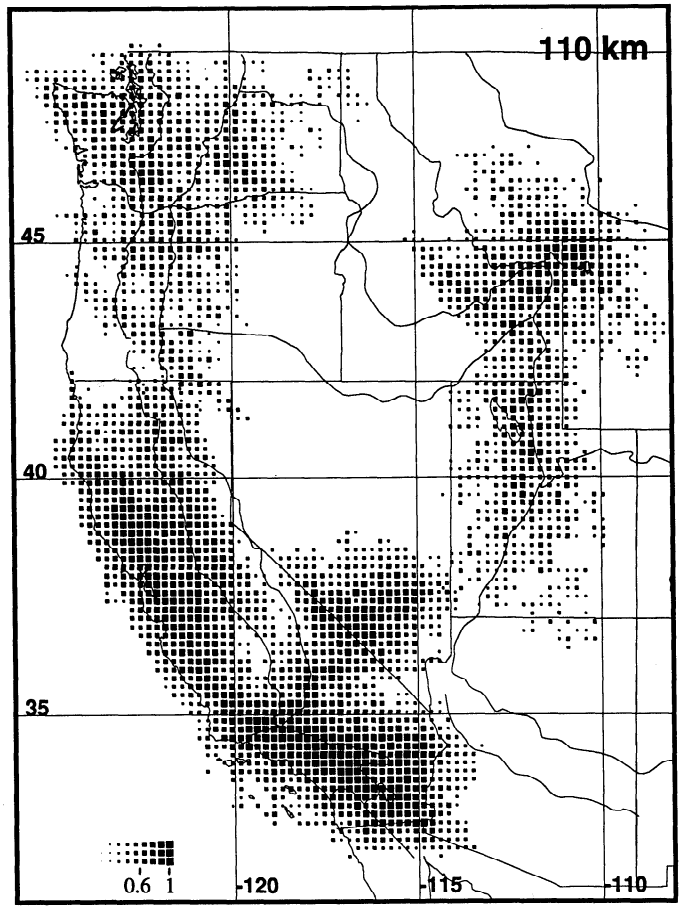

Fig. 6. Hit quality at 110 km depth. For each model parameter, hit quality is determined by taking the weighted average of the number of rays sampling the four delta/azimuth bins shown in Figure 3 plus one for the core phases. Each bin is considered filled if four or more rays are present; therefore a hit quality of one (maximum symbol size) requires at least four rays in each of the five bins. From experience, model parameters with a hit quality above 0.6 usually are well resolved and insensitive to noise.

UPPER MANTLE *P* WAVE STRUCTURE

The rays recorded by each of the three array clusters do not share significant volumes of upper mantle above 400 km. Therefore, the data sets from each of the clusters are inverted separately. The three resulting images are superimposed to make a regional map of the upper mantle structure. To account for the small average velocity differences that exist among the various clusters (Table 4), a corresponding velocity adjustment is added to each inversion. Because the addition of any horizontally layered structure that causes the proper delay will suffice, the depth distribution of this structure must be based on independent information. For the following reasons, we assume that major lateral variations in upper mantle structure lie above 200 km. In regions of good resolution, imaged structure resides primarily above ~200 km. In regions of poorer resolution, where the maximum depth of structural heterogeneity is not well constrained, travel time delays are similar in magnitude to those from regions of better resolution and hence are consistent with this depth being no greater than 200 km. Furthermore, the presence of most upper mantle heterogeneity contained within the upper 200 km is consistent with stochastic modeling of the ISC data set [*Gudmundsson et al.*, 1990]. Average velocities for each mantle layer above 200 km are adjusted to account for the differences in average arrival time among clusters. These differences are small, indicating that average delays to these western U.S. arrays are not significantly different. The difference between the Pacific Northwest array cluster and the California array cluster is the largest; at 0.15 s this time shift results in increased Pacific Northwest upper mantle velocities above 200 km of ~0.7% in relation to California upper mantle. Average upper mantle beneath the eastern Great Basin cluster is estimated to be ~0.4% faster than the California upper mantle. The important point is that the values of these velocity adjustments are small.

Many inversions have been performed in order to understand the effects of model parameterization, smoothing and iteration number on the final image. Although details of the resultant images differ among these inversions, the features discussed in this paper are invariant with respect to these changes. The model presented below consists of cubes 20 km on a side extending in depth to 400 km. Ten iterations are applied, resulting in a RMS residual reduction of ~50%, or a variance reduction of ~75% (Table 1). Figure 9 shows the resulting inversion of the *P* wave data for upper mantle structure.

We divide the western United States into a marginal domain and an interior domain based on uppermost mantle structure

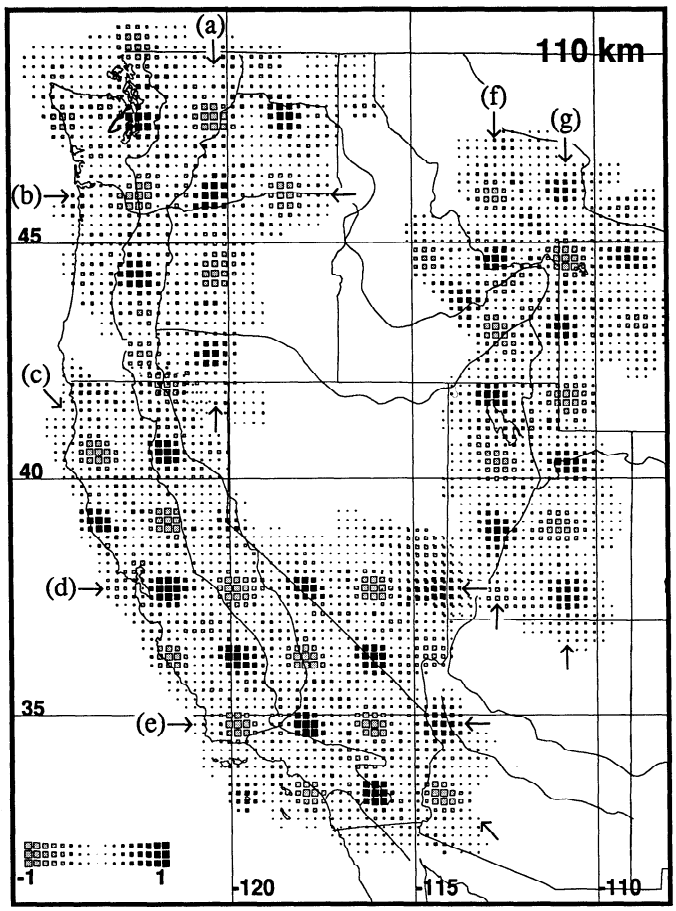

Fig. 7. Map view of test structure image. To test spatial resolution, inversion is performed on data created by calculating delays that result from a specified structure. This structure consists of vertical "posts" confined entirely between the depths of 40 and 200 km (i.e., no anomaly is input in the "crust" or below 200 km). The anomalous posts, of a cross section of 3 by 3 blocks (i.e., 60 × 60 km) and alternating anomaly value, are embedded in a nonanomalous background. Inversion tests both lateral resolution in the upper 200 km and the degree of vertical streaking of structure from the upper 200 km into the lower 200 km. Full symbol size indicates 100% reconstruction of input amplitude. At 110 km depth, the input structure is located well and amplitude reconstruction is nearly complete in the well-sampled regions. Cross-section locations (a)-(g) (for Figures 8a-8g) are shown.

shown in Figure 9, as well as average elevation, the occurrence of young volcanism, and tectonic style. The marginal domain lies within ~250 km of the Pacific coastline, where the orientation of the long-wavelength upper mantle features at 70 and 110 km depth (Figure 9; major features are listed in Table 5) generally are concordant with the major young tectonic and physiograghic structures. Elevations there are relatively low, and tectonism occurs at relatively high rates and is dominated by plate interactions (strike-slip faulting south of the Cape Mendocino and subduction to the north). Within the interior domain, uppermost mantle structures trend northeasterly and generally are discordant with the young tectonic structures but are concordant with young volcanic activity. The interior domain stands at high average elevations compared to the margin, and tectonism occurs at a low rate and is dominated by normal faulting. The area that includes the high Sierra Nevada and the western Great Basin expresses attributes common to both domains. This zone appears to be one of transition.

In the following sections, we identify what we consider to be authentic, major upper mantle seismic structures (Table 5). Our

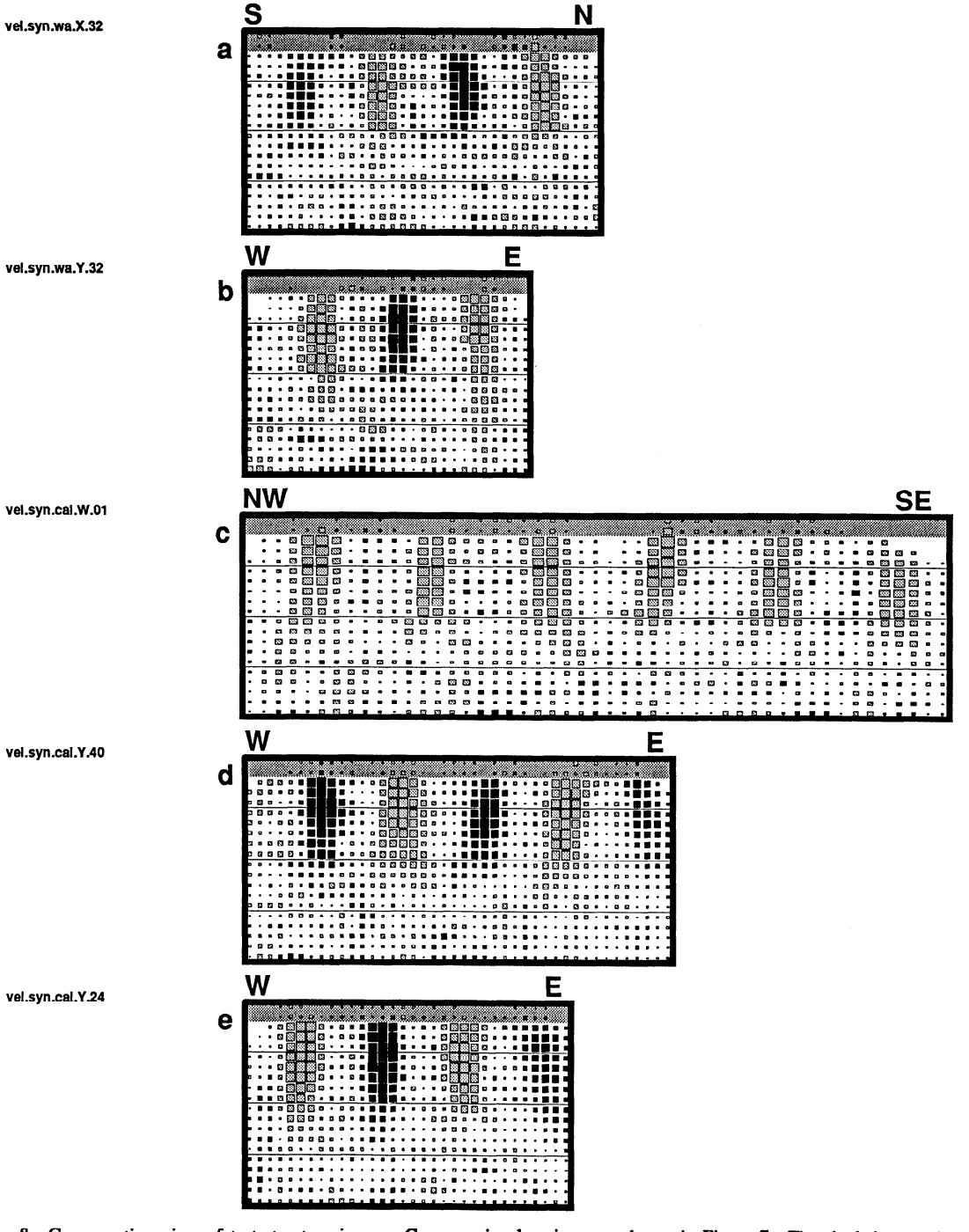

Fig. 8. Cross section view of test structure image. Cross section locations are shown in Figure 7. The shaded upper layer represents the portion of the inversion modeled as the crust (see text). The fine horizontal lines are spaced at 100 km intervals. These cross sections show the spatial characteristics of artifacts created by imperfect reconstruction of the input structure. In general, the lateral resolution of the input structure is good, whereas depth resolution varies. Based on these images, we argue that upper mantle structure above 200 km depth can be resolved well in most areas and that moderate amounts of artifact in the 200-400 km depth range can be created by downward streaking of structure present above 200 km.

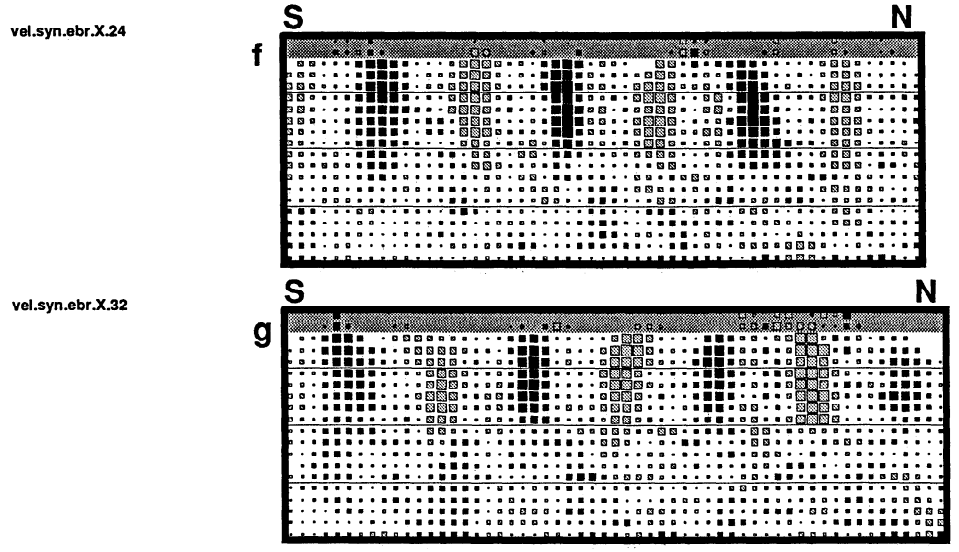

Fig. 8. (continued)

identification of upper mantle seismic structures is based on the structure seen in the maps at 70 and 110 km depth. We have chosen these depths because the imaged features in cross section generally define continuous bodies extending to these depths from the base of the crust; and this is the depth range of best resolution.

Uppermost Mantle Structures of the Marginal Domain

1. Relatively high-velocity upper mantle is imaged beneath westernmost California and the offshore region, extending south from near Cape Mendocino to the San Francisco Bay region (BA in Table 5). This feature lies in a region through which the Farallon slab and associated subplates recently subducted [*Fernandez and Hey*, 1991] and presently should be in the region of the "slab-free window" created as the Mendocino triple junction migrated north to Cape Mendocino [*Dickenson and Snyder*, 1979]. This feature might represent oceanic lithosphere that has been thrust beneath the margin of North America, either pieces of the Farallon plate that were not carried away as the rest of this plate subducted or oceanic lithosphere more recently underthrust, associated with shortening near the California margin.

2. A large volume of low-velocity upper mantle lies beneath the Coast Ranges, extending from the westernmost Transverse Ranges north to the Olympic Mountains. This low-velocity volume also includes the western margins of the adjoining forearc sedimentary basins: the western Puget Trough/Willamette Valley (west of the Cascade volcanic arc) and the western Great Valley. The magnitude of this low-velocity feature is most anomalous beneath the Olympic Mountains and northern California, where the upper mantle velocities are among the lowest in the inversion. Beneath the Olympic Mountains and the Coast Ranges of the Pacific Northwest, upper mantle velocities must be low enough that arrivals are late in spite of the fact that they traverse the subducted Juan de Fuca slab, which is nearly horizontal there (and hence unresolvable with teleseismic rays). The low velocities beneath northern California Coast ranges (CCR) probably represent the slab-free window created as the Juan de Fuca and Gorda slabs withdraw to the north [*Benz et al.*, 1992]. Consistent with this interpretation, the magnitude of this anomaly increases north of the Mendocino triple junction. However, significant variations in velocity occur that are not easily interpreted by simple models of slab removal. The most prominent of such variations is the the zone of moderate velocity seen at 70 km depth that extends west of San Francisco Bay.

3. The steeply dipping Juan de Fuca (JDF) and Gorda slabs (GS) are imaged beneath the Cascades volcanic arc. The magnitude of this high-velocity structure depends on position, with structure being less pronounced beneath the Columbia River and beneath southern Oregon. The slab is well resolved beneath central Washington, where the image of the subducted Juan de Fuca slab extends to about 300 km depth [*Rasmussen and Humphreys*, 1988]. Beneath southern Oregon the slab appears to penetrate to depths of at least 200 km [*Harris et al.*, 1991]. Resolution of the Gorda slab is poor beneath northeastern California, though the great magnitude of the residuals suggests that this slab may extend to depths at least as great as the the Juan de Fuca slab beneath Washington. Above 120 km, the high-velocity anomaly attributed to subducted slab beneath the Pacific Northwest extends south as a continuous feature as far as the southern Great Valley. Indeed, this high-velocity structure is the most prominent feature imaged in our inversion. At 150 km depth, this feature is separated into a northern part (the Gorda slab, GS) and a southern part (southern Great Valley, sGV) [*Biasi and Humphreys*, 1992]. The origin of the sGV structure is not clear, but it may be abandoned fragments of the older Farallon plate or downwelling of (North American) mantle lithosphere [*Biasi and Humphreys*, 1992].

4. An east trending high-velocity feature lies beneath the Transverse Ranges of southern California (TR). The base of this structure is resolved near 100 km depth on its western end, and near 240 km depth on its eastern end [*Humphreys and Clayton*, 1990]. This feature is interpreted as downwelling lithosphere, consistent with crustal convergence in the Transverse Ranges [*Bird and Rosenstock*, 1984; *Sheffels and McNutt*, 1986; *Humphreys and Hager*, 1990].

5. The region beneath the Salton Trough (ST) is slow. The Salton Trough, as the northern terminus of the East Pacific Rise, is considered to be rifting lithosphere. Its location near the Transverse Ranges downwelling defines a local convection cell that controls local tectonic activity [*Humphreys and Hager*, 1990].

Uppermost Mantle Structures of the Interior Domain

Based on our upper mantle images and additional seismic information (for those regions where we do not have a tomographic inversion, which are discussed in the following section),

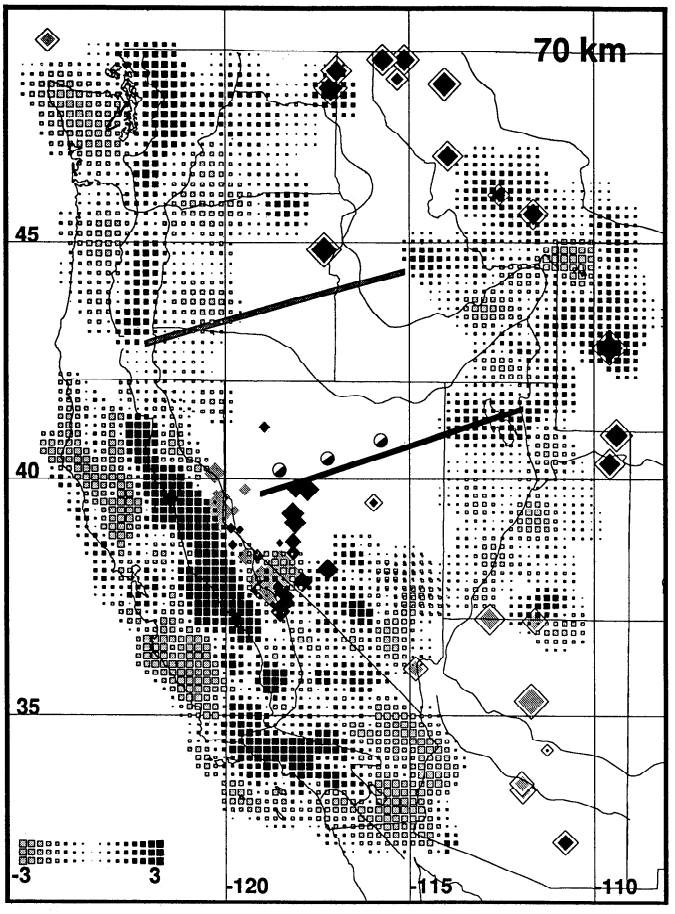

Fig. 9. Tomographic image of V_P structure at the indicated depths. Solid and shaded symbols represent regions of fast and slow velocities, respectively, with symbol size being proportional to velocity perturbation. Imaged velocities deviate by approximately ±4% within resolvable volumes. In this figure, full symbol size represents velocity perturbations greater than ±3%. The model depth is 400 km, with each model block occupying a cube measuring 20×20×20 km. Lateral resolution of the structures imaged generally is very good (see Figure 7). Some of the additional upper mantle velocity indicators from Figure 3 are shown on the map of structure at 70 km depth, where the largest symbols represent teleseismic delays of ±1 s. Cross-section locations (a)-(m) (for Figures 10a-10m) are shown on the map of structure at 110 km depth. For reference, province boundaries are shown.

we identify basic structural trends beneath the western U. S. interior. This structure consists of two elongate, northeast trending low-velocity structures that are at least partly surrounded by high-velocity upper mantle.

1. The northernmost low-velocity trend is imaged beneath the Yellowstone caldera and the eastern Snake River Plain (eSRP in Table 5), and extends southwest to the Carson Sink. Resolution of this feature is good beneath the eastern Snake River Plain, where a volume of low velocities confined to a narrow northeast trending zone (60-100 km wide) is imaged to depths of 150-200 km [*Iyer et al.*, 1981; *Evans*, 1982; *Dueker and Humphreys*, 1990]. Recent efforts to more accurately resolve the depth extent of this anomalous mantle indicate that it extends 150±50 km beneath Yellowstone and 200±50 km beneath southeastern Idaho [*Dueker and Humphreys*, in prep.]. The western end of this low-velocity volume is quite wide, underlying the Great Basin of northwest Nevada and southeast Oregon [*Dueker and Humphreys*, 1990].

2. The more southerly low-velocity trend, termed the St. George volcanic trend (SGVT), lies beneath the region extending from southern Nevada to central Utah, where it ends beneath the Colorado Plateau. Although this feature is poorly resolved, its location is substantiated by a pattern of late arrivals observed in Figure 3, especially for arrivals from the southwest.

3. A high-velocity volume of upper mantle lies between these two low-velocity zones, extending southwest from west central Wyoming across northern Utah, the Wasatch Front and Sevier Depression, and into the central Great Basin (cGB). The southeastern margin of this feature can be traced southwest across central Utah and southern Nevada to near the California border, where it has been associated with the removal of partial melt near the early Tertiary Timber Mountain Caldera [*Spence*, 1974; *Monfort and Evans*, 1982].

4. High velocities are imaged beneath the northeastern Washington (Okanogan highlands, OK) and the eastern Washington-Oregon boundary area (Blue Mountains, BM).

Depth Extent of Mantle Structure

The map view images of upper mantle V_P structure illustrate the heterogeneous nature of the western U.S. upper mantle. The ability to locate lateral upper mantle velocity transitions with the use of teleseismic rays is excellent, and the variations observed in Figure 9 are authentic. In contrast to the lateral structure, resolution in the vertical direction is relatively poor and the cross sectional images shown in Figure 10 are not as reliable. In general, only the regions within the interior of an array will have enough crossing rays to constrain the depth extent of velocity perturbations, and even there the vertical elongation of resolution kernels will tend to spread structure vertically. Thus, even in the most resolved regions, interpretation of the base of an imaged feature is inherently ambiguous. Examination of the resolution test (Figure 8) shows that in the well-sampled regions, the volume of imaged anomalous velocity associated

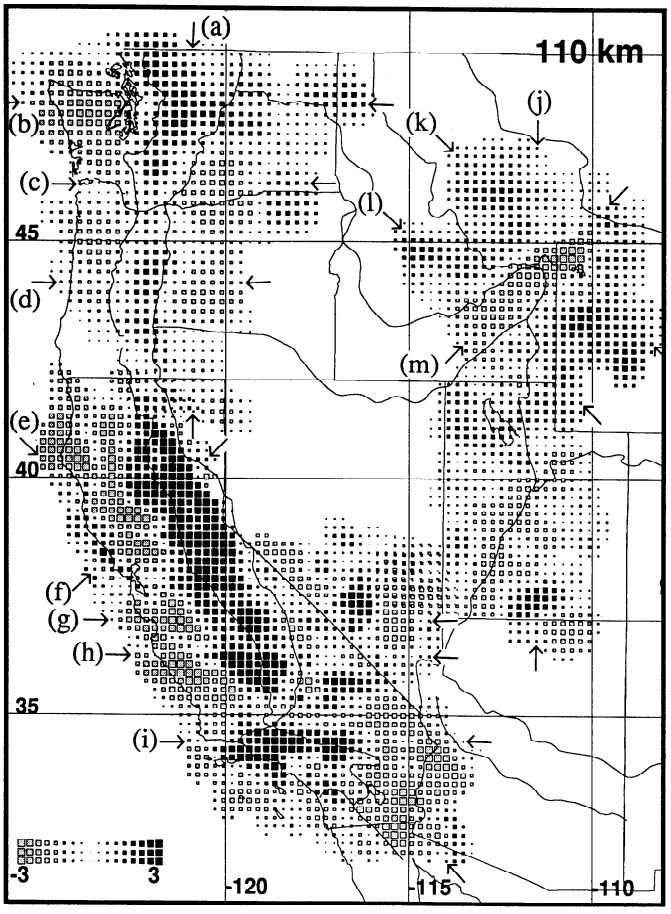

Fig. 9. (continued)

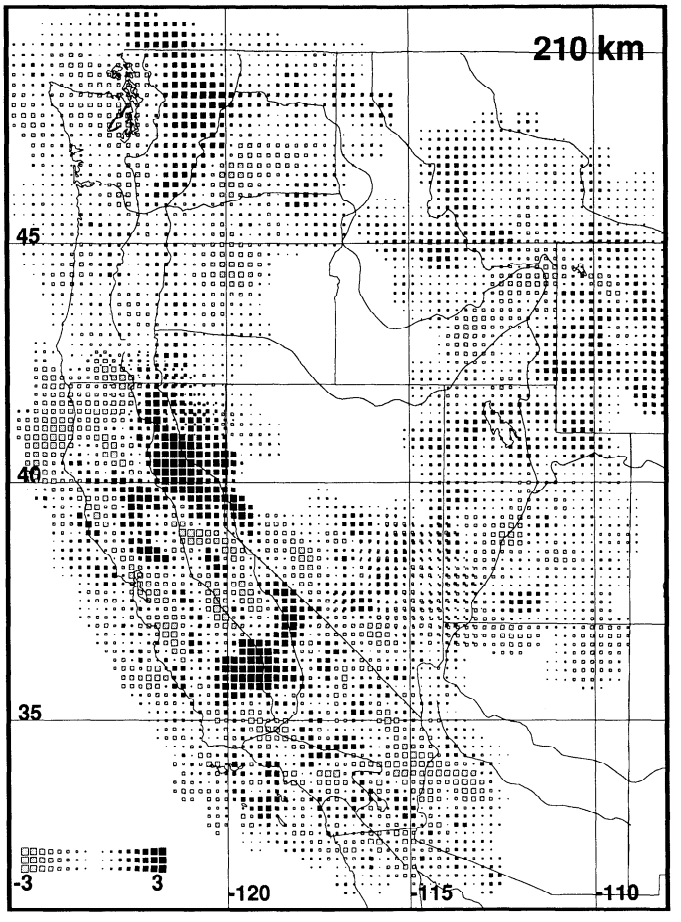

Fig. 9. (continued)

with the 200-km-deep posts is streaked down beyond the base of the posts by 20-100 km. In practice, we infer that a coherent upper mantle feature lies above the depth where the magnitude of that feature diminishes rapidly with depth. Using this as a guide works well for the inversions of synthetic data and if we apply this rule of thumb to the inversion of actual data, most of the velocity structure reconstructed in the 200-400 km depth range can be attributed to structure above 200 km depth.

The structures identified in Table 5 are shown in cross section in Figure 10. Figure 10a shows the variable velocity structure of the Cascadia back arc upper mantle, with relatively high velocities present beneath northern Washington (OK) and low velocities beneath southern Washington and Oregon. The image of the subducting Juan de Fuca slab (JDF) is shown in Figures 10b-10d. The slab to the south appears to be of lesser magnitude than it does to the north, although the contrast between the slab and the back-arc upper mantle (which is the most resolvable aspect of this feature) remains strong. Figure 10e trends SE from the Cape Mendocino region, crossing the high-velocity southern Great Valley (sGV) structure, the Transverse Ranges (TR), and the slow upper mantle in the upper ~100 km beneath the Salton Trough (ST). In northern California, Figure 10f shows slightly high-velocity upper mantle extending beneath the California coastal region (BA), low velocities attributed to the slab-free window extending about 150 km beneath the northern California Coast Ranges (nCCR) and the prominent Gorda slab (GS) extending to a depth of at least 300 km. Cross sections farther south (Figure 10g and 10h) shows the slab-free window beneath the Coast Ranges, the high velocities beneath the southern Great Valley (sGV) extending to depths of 200-300 km and the neutral velocities beneath the high-standing eastern Sierra Nevada. Figure 10g also shows the high velocities velocities of the central Great Basin (cGB), which in the Timber Mountain Caldera region appear to extend to 100-200 km depth, and the low velocities beneath southern extension of the St. George volcanic trend (SGVT). Figure 10i crosses the high-velocity Transverse Ranges (TR) structure, which extends to a depth of about 200 km on its eastern end.

Figure 10j crosses both the Yellowstone and St. George low-velocity trends, as well as the relatively high-velocity upper mantle that separates these trends. Low velocities associated with the St. George trend appear to extend to about 100 km depth, though resolution there is poor. In the Yellowstone region, Figure 10k shows a 100-km-wide low-velocity body beneath the Yellowstone Caldera which extends to depths of 100-140 km. These low velocities represent the northeasterly extent of the low velocity volume present beneath the length of eastern Snake River Plain (eSRP). As shown in Figures 10l and 10m, velocities beneath the Snake River Plain are not as low as those beneath the Caldera but extend to greater depths.

ADDITIONAL INFORMATION ON SEISMIC STRUCTURE

With varying degrees of resolution, the structure of much of the western U.S. upper mantle is presented in this study. However, large volumes of the interior domain upper mantle are unsampled by our ray set. By using other seismic studies, large-scale aspects of the upper mantle seismic structure can be extended into these regions.

Interior Domain

The lateral transition in upper mantle structure between the low velocities of the eastern Snake River Plain and the high velocities to the southeast is well resolved in our inversion.

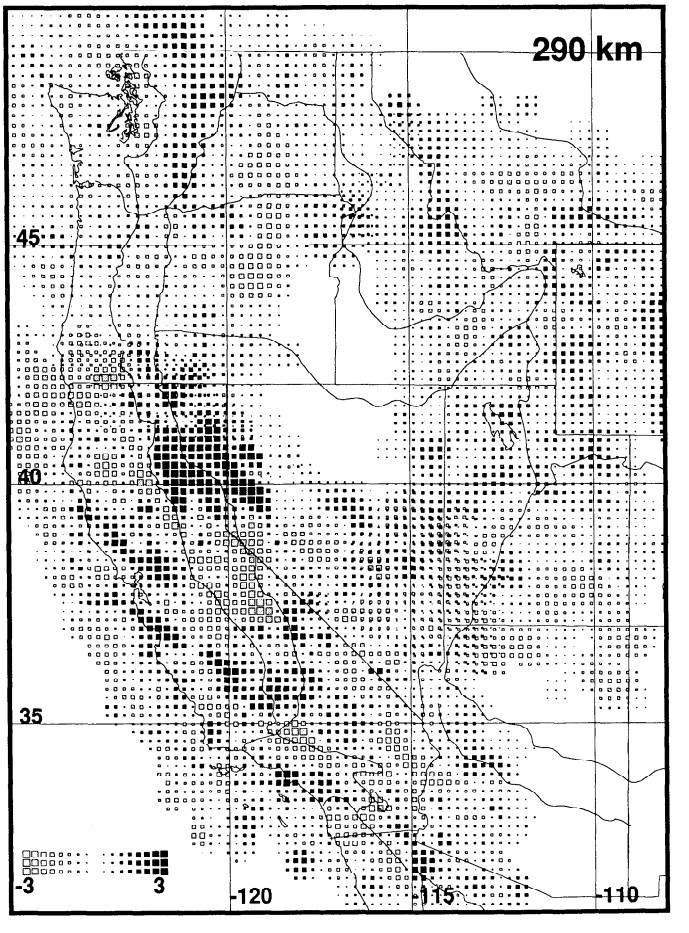

Fig. 9. (continued)

TABLE 5. Western U.S. Upper Mantle V_P Features

Label	Feature†	Velocity	Depth*, km	Possible Origin	References
BA	Bay Area (central California)	fast	100±50	underthrust slab	1
BM	Blue Mountains	fast	?	thick lithosphere or melt extraction	2
cGB	Central Great Basin	fast	?	melt extraction	4
nCCR	N. Calif. Coast Ranges	slow	100±50	MTJ migration	1
eSRP	Eastern Snake River	slow	175±50	active magmatism	5
GS	Gorda Slab (NW California)	fast	>300	subduction	1
JDF	Juan de Fuca Slab	fast	>150-300	subduction	3
JVT	Jemez volcanic trend	slow	?	active magmatism	6
OK	Okanogan Highlands	fast	100-200	thick lithosphere or melt extraction	2
SGVT	St. George volcanic trend	slow	?	active magmatism	4
ST	Salton Trough	slow	100±50	passive rift	7
sGV	Southern Great Valley	fast	200-300	abandoned slab and/or	8
				lithospheric downwelling	8
TR	Transverse Ranges	fast	240±50	lithospheric downwelling	7

References: 1, *Zandt* [1981], *Benz et al.* [1992]; 2, *Rasmussen and Humphreys* [1988]; 3, *Iyer and Rite* [1981], *Michealson and Weaver* [1986], *Rasmussen and Humphreys* [1988]; 4, *Dueker and Humphreys* [1990]; 5, *Iyer et al.* [1981], *Evans* [1982]; 6, *Parker et al.* [1984], *Spence and Gross* [1990]; 7, *Raikes* [1980], *Humphreys and Clayton* [1990]; 8, *Humphreys and Clayton* [1990], *Jones et al.* [in press], *Biasi and Humphreys* [1992].

†See Figure 2 and text for locations.

*Depth to base of feature.

Additional seismic evidence from the Great Basin suggests that this transition continues southwest across central Nevada to near the California-Nevada border [*Dueker and Humphreys*, 1990], where it terminates against the northwest trending region of relatively low velocities beneath the westernmost Great Basin. The approximate position of this transition in northern Nevada is inferred by noting the strong azimuthal variations in teleseismic P wave residuals observed at three stations located near this transition (Figure 4). Relatively early arrivals (~1 s) are observed from the southeast relative to arrivals from the northwest [*Koizumi et al.*, 1973]. A temporary deployment of seismometers in this region (see Figure 4 for station locations) recorded similar azimuthal patterns of teleseismic arrivals, which have been interpreted as indicative of deep (~200 km) high-velocity upper mantle to the southeast [*Iyer et al.*, 1977; Iyer, personal communication, 1991]. Surface wave studies from this region allow us to infer a more regional sense of the average upper mantle velocities. Upper mantle velocities along a line predominately in southeastern Oregon are found to average ~8% slower than the upper mantle in the Great Basin just south of the transition (see Figure 4 for locations) [*Priestley and Brune*, 1978, 1982]. Thus the volumes of high- and low-velocity upper mantle appear to extend away from the upper mantle transition in central Nevada for 100 km or more (although it seems likely that the small-scale structure beneath each of these regions is heterogeneous, based on the heterogeneous nature of structure resolved elsewhere).

A northeast trending volume of low-velocity upper mantle has been observed beneath the portion of the southwestern Colorado Plateau [*York and Helmberger*, 1973] that corresponds with late teleseismic arrivals to stations in this region (seen especially in Figure 4). In addition to the northeast trending low-velocity upper mantle volumes associated with the Snake River Plain and St. George volcanic trend, a third northeast trending low-velocity trend exists beneath the Jemez volcanic trend (JVT in Table 5) in New Mexico [*Parker et al.*, 1984; *Spence and Gross*, 1990; *Davis et al.*, 1993]. This volume of low-velocity upper mantle defines a feature that is more prominent than the seismic structures associated with the Rio Grande Rift [*Spence and Gross*, 1990; *Davis et al.*, 1993].

Hearn et al. [1991] investigated the uppermost western U.S. mantle with P_n arrivals that have traveled horizontally beneath the Moho in the upper 10-20 km of the mantle. This provides an independent means of examining some of the same volumes of upper mantle. Interpretation of P_n refraction velocity can be complicated by an irregular Moho topography, which can influence travel times in ways that are difficult to distinguish from variations in upper mantle velocity. However, this is not expected to be a problem in the Great Basin region because the Moho there is thought to be flat and horizontal [*Mooney and Braile*, 1989; *Thompson et al.*, 1989]. Within the interior domain, the upper mantle images provided by our study and Hearn et al.'s study are very similar. This suggests that the teleseismically imaged upper mantle velocity structure extends up to the Moho. Noteworthy is the presence of the northeast trending Great Basin high-velocity feature in both studies.

The occurrence of upper mantle anisotropy beneath the western United States is well established, often causing ~1 s split in shear wave arrivals [*Silver and Chan*, 1988; *Savage et al.*, 1990]. Hence it is reasonable to ask what fraction of the teleseismic P delays are caused by anisotropy. Unlike S waves, teleseismic P wave residuals would be most affected by an alignment that has the fast axis dipping ~45°. This alignment could create significantly different velocities for teleseismic arrivals of opposing backazimuths. The effect of anisotropy on our inversion is thought to be relatively minor for three reasons: (1) the sort of azimuthal variations in teleseismic delay that would be created by anisotropic upper mantle are not apparent in Figure 3, (2) inversions of this data set using a tomographic algorithm that suppresses the affects of anisotropy by averaging delays from the four azimuthal quadrants creates upper mantle images very similar to those obtained here [*Dueker and Humphreys*, 1992], and (3) the upper mantle structure inferred with near-horizontal P_n arrivals [*Hearn et al.*, 1991] and with roughly vertical teleseismic arrivals is similar.

Marginal Domain

The P_n structure in the marginal domain [*Hearn et al.*, 1991] is not well correlated with upper mantle velocity structure imaged with teleseismic data. This poor correlation is in contrast to the good correlation discussed above for the continental interior. However, it is considered genuine in light of the abundant high-quality teleseismic and P_n data from this area. Apparently, either the uppermost mantle structure imaged with P_n phases is considerably different from the structure we image in the upper tens of kilometers of the mantle, or Moho topography is influencing the P_n travel times [*Mooney and Weaver*, 1989]. *Hearn et al.* [1991] suggest that Moho topography is

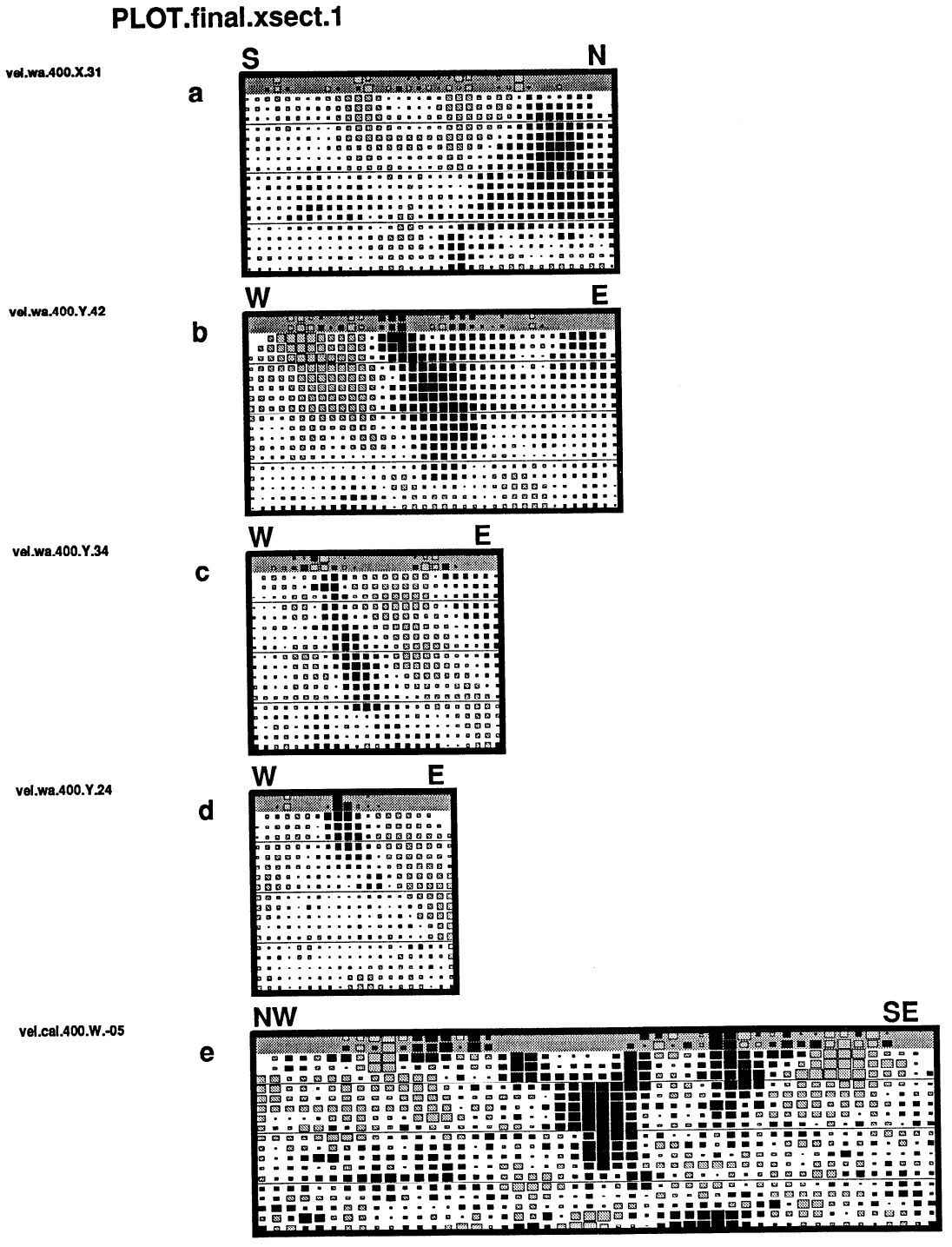

Fig. 10. Cross sections of tomographically imaged V_P structure. Cross section locations are shown in Figure 9. Solid and shaded symbols represent regions of fast and slow velocities, respectively. Symbol size is proportional to velocity perturbation, with full symbol size representing a ±3% velocity perturbation. The shaded upper layer represents the portion of the inversion modeled as the crust (see text). The fine horizontal lines are spaced at 100 km intervals. One should be aware that resolution varies considerably from location to location and that downward "streaking" of the actual structure often occurs in reconstructions that use teleseismic data (see Figure 8).

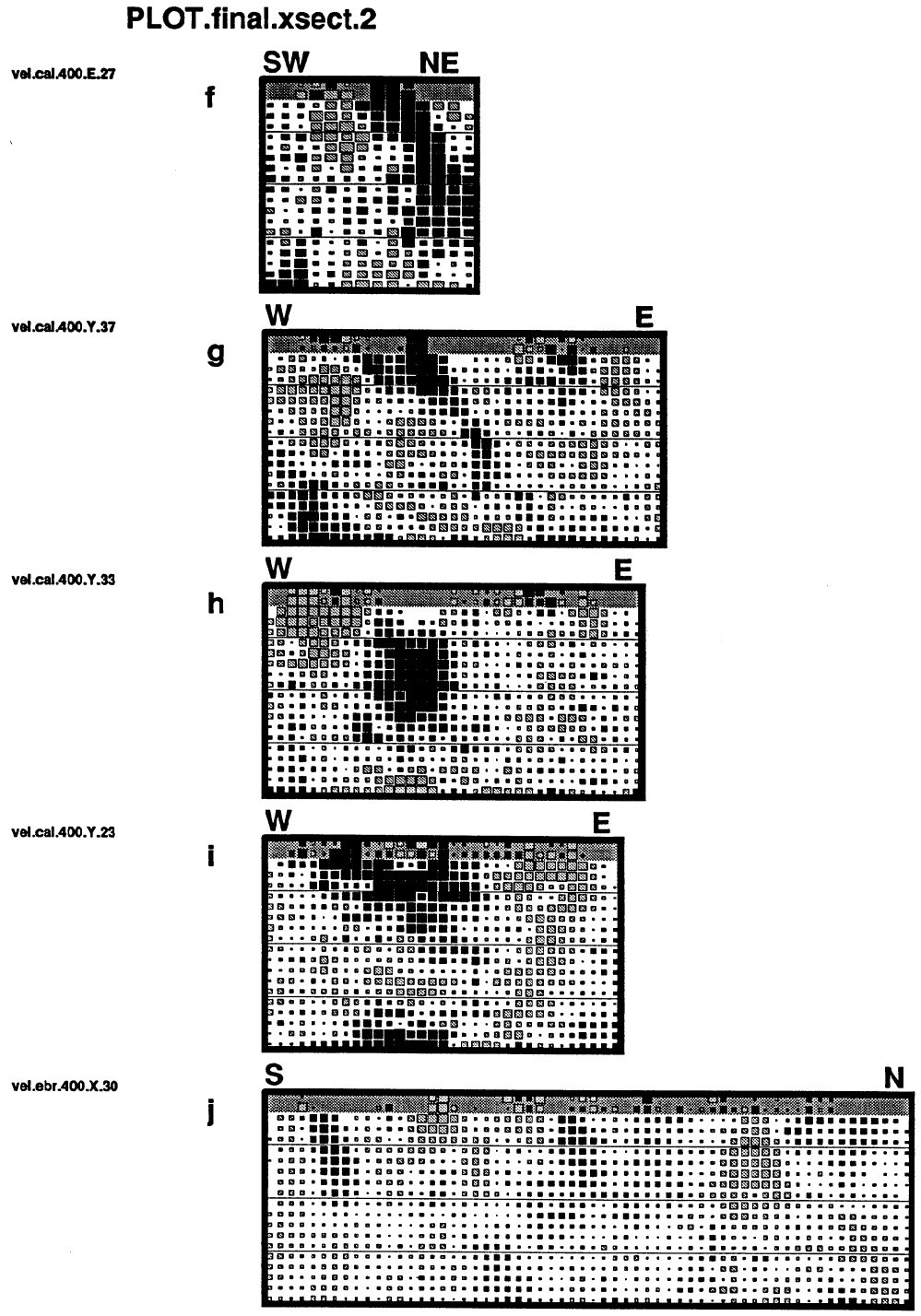

Fig. 10. (continued)

responsible for the slow apparent P_n velocities beneath the Sierra Nevada.

Region of Transition

Late arrivals to University of Nevada stations near the California border contribute to defining a northwest trending zone of relatively low velocities lying east of the Sierra Nevada (diamond symbols in Figure 4). Although station coverage in this region is sparse, it is complete enough to suggest that the southwest trending zone of high velocities found beneath the Great Basin does not merge with the high-velocity region beneath the north and central Sierra Nevada (Figure 9 and Figure 10g) [*Jones et al.*, 1993; *Biasi and Humphreys*, 1992]. We consider this region of lower mantle velocity, which coincides with the Walker Lane Belt [*Stewart*, 1988], to be transitional between the interior and marginal domains because it shares characteristics of both the marginal domain (northwest orientation of upper mantle structure and an association with tectonic activity) and the interior domain (high average elevations and active volcanism). The style of faulting there shares characteris-

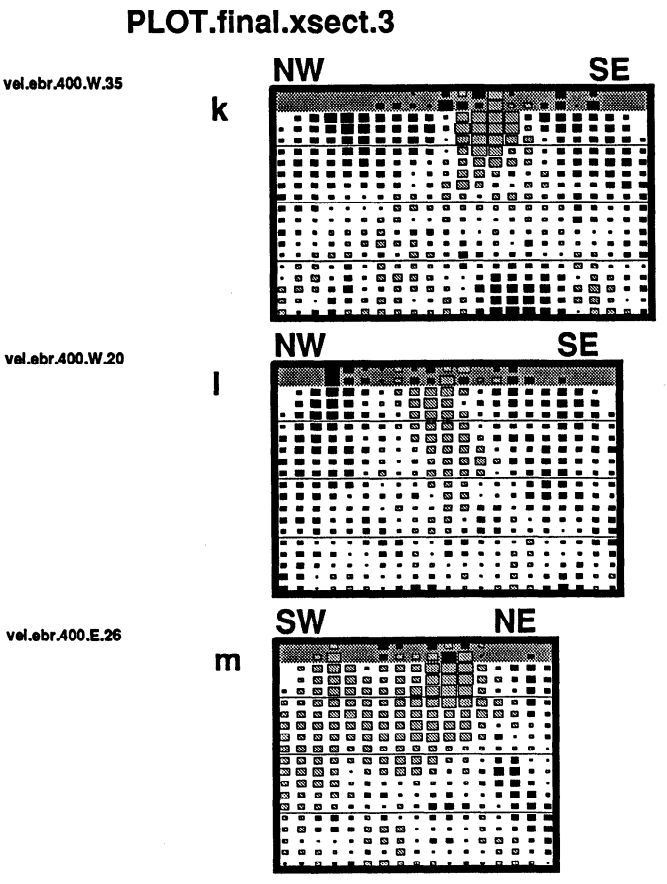

Fig. 10. (continued)

tics from both domains as well (i.e., important components of both strike-slip and normal faulting).

CONCLUSIONS

The average upper mantle beneath the western United States is slow, delaying P wave arrivals by ~0.6 s compared to global average [*Dziewonski and Anderson*, 1983]. Western U.S. upper mantle studies that resolve the depth-varying part of the structure find a well-developed low-velocity zone between 50 and 200 km depth [*Iyer and Hitchcock*, 1989; *Grand*, 1987]. V_P structure shown in this paper deviates from average by about ±4%, defining a heterogeneous structure that appears to reside primarily within the upper few hundred kilometers of the mantle (except for the subducted Juan de Fuca and Gorda slabs). Thus the heterogeneity that we image resides largely within the low-velocity zone deduced with data that resolve the laterally averaged depth structure.

The lateral contrasts in upper mantle V_P structure that we image can be extended to regions where array data do not exist by using other seismic studies to produce a fairly complete view of the upper mantle beneath the western United States (at least for scale lengths greater than about 100 km). Based on a combination of the upper mantle structure, tectonic province, and average elevation, the western United States is divided into two major regions: (1) Within ~250 km of the North American coastline are found relatively low elevations, transform- or subduction-related tectonics, and elongated, northwest oriented volumes of alternating high- and low-velocity upper mantle of wavelength ~250 km that generally parallel the physiographic and tectonic grain of the region. (2) Within the western U.S. interior are found relatively high elevations, extension-dominated tectonics, and southwest oriented volumes of alternating high- and low-velocity upper mantle of wavelength ~500 km that are discordant with physiographic and tectonic province but are associated with the young volcanism of the Yellowstone, St. George, and Jemez trends. A transition region between these two domains corresponds well with the tectonically and volcanically active Walker Lane belt.

Acknowledgments. This research was funded under NSF grant EAR-8804953. We appreciate thoughtful reviews by Walter Mooney, Steve Roecker, and Brian Mitchell, which improved the quality of this paper. The 44,000 P wave arrivals delays which comprise this data set derive from the work of Glen Biasi, Sue Raikes, H.M. Iyer, John Evans, George Zandt, Robert Cockerham, Caryl Michaelson, Dave Oppenheimer, Jim Pechmann, John Rasmussen, and ourselves; our thanks to all who shared data with us.

REFERENCES

Al-Katib, H. H., and B. J. Mitchell, Upper mantle anelasticity and tectonic evolution of the western United States from surface wave attenuation, *J. Geophys. Res.*, *96*, 18,129-18,146, 1991.

Archambeau, C. B., E. A. Flinn, and D. G. Lambert, Fine structure of the upper mantle, *J. Geophys. Res.*, *74*, 5825-5865 1969.

Benz, H. M., G. Zandt, and D. H. Oppenheimer, Lithospheric structure of northern California determined from teleseismic images of the upper mantle, *J. Geophys. Res.*, *97*, 4791-4808, 1992.

Biasi, G. P., and E. D. Humphreys, P-wave image of the upper mantle structure of central California and southern Nevada, *Geophys. Res. Lett.*, *19*, 1161-1164, 1992.

Bird, P., and R. W. Rosenstock, Kinematics of present crust and mantle flow in southern California, *Geol. Soc. Am. Bull.*, *95*, 946-957, 1984.

Burdick, L. J., and D. V. Helmberger, The upper mantle velocity structure of the western United States, *J. Geophys. Res.*, *83*, 1699-1712, 1978.

Cleary, J., and A. L. Hales, An analysis of the travel times of P waves to North American stations in the distance range 30° to 100°, *Bull. Seismol. Soc. Am.*, *56*, 467-489, 1966.

Davis, P. M., P. Slack, H. A. Dahlheim, W. V. Green, R. P. Meyer, U. Achauer, A. Glahn, and M. Granet, Teleseismic tomography of continental rift zones, in *Seismic Tomography: Theory and Practice*, edited by H. M. Iyer and K. Hirahara, pp. 397-439, Blackwell, London, 1993.

Dickenson, W. R., and W. S. Snyder, Geometry of subducted slabs related to the San Andreas transform, *J. Geol.*, *87*, 609-627, 1979.

Dueker, K. G., and E. D. Humphreys, Upper-mantle velocity structure of the Great Basin, *Geophys. Res. Lett.*, *17*, 1327-1330, 1990.

Dueker, K. G., and E. D. Humphreys, Teleseismic imaging of the western United States upper mantle structure using the Simultaneous Iterative Reconstruction Technique, in *Seismic Tomography: Theory and Practice*, edited by H. M. Iyer and K Hirahara, pp.265-298, Blackwell, London, 1993.

Dziewonski, A. M., and D. L. Anderson, Preliminary reference Earth model (PREM), *Phys. Earth Planet. Inter.*, *25*, 297-356, 1981.

Dziewonski, A. M., and D. L. Anderson, Travel times and station corrections for P-waves at teleseismic distances, *J. Geophys. Res.*, *88*, 3295-3314, 1983.

Evans, J. R., Compressional wave velocity structure of the upper 350 km under the eastern Snake River Plain near Rexburg, Idaho, *J. Geophys. Res.*, *87*, 2654-2670, 1982.

Fernandez, L. S., and R. N. Hey, Late Tertiary tectonic evolution of the seafloor spreading system off the coast of California between the Mendocino and Murray fracture zones, *J. Geophys. Res.*, *96*, 17,955-17,979, 1991.

Gomberg, J., K. Priestley, and J. Brune, The compressional velocity structure of the crust and upper mantle of northern Mexico and the border region, *Bull. Seismol. Soc. Am.*, *79*, 1496-1519, 1989.

Grand, S. P., Tomographic inversion for shear structure beneath the North American plate, *J. Geophys. Res.*, *92*, 14,065-14,090, 1987.

Grand, S. P., A possible bias in travel time measurements reported to ISC, *Geophys. Res. Lett.*, *17*, 17-20, 1990.

Grand, S. P., and D. V. Helmberger, Upper mantle shear structure of North America, *Geophys. J. R. Astron. Soc.*, *76*, 399-438, 1984.

Gudmundsson, O., J. H. Davies, and R. W. Clayton, Stochastic analysis of global travel time data: Mantle heterogeneity and random errors in the ISC data, *Geophys. J. Int.*, *102*, 25-43, 1990.

Hales, A. L., Upper mantle models and the thickness of the continental lithosphere, *Geophys. J. Int., 105*, 355-363, 1991.

Hales, A. L., and J. R. Doyle, *P* and *S* travel time anomalies and their interpretation, *Geophys. J. R. Astron. Soc., 13*, 403-415, 1967.

Hales, A. L., J. R. Cleary, H. A. Doyle, R. Green, and J. Roberts, *P* wave station anomalies and the structure of the upper mantle, *J. Geophys. Res., 73*, 3885-3896, 1968.

Harris, R. A., H. M. Iyer, and P. B. Dawson, Imaging the Juan de Fuca plate beneath southern Oregon using teleseismic *P* wave residuals, *J. Geophys. Res., 96*, 19,879-19,889, 1991.

Hearn, T. M., and R. W. Clayton, Lateral velocity variations in southern California, II, Results for the lower crust from P_n waves, *Bull. Seismol. Soc. Am., 76*, 511-520, 1986.

Hearn, T. M., N. Beghoul, and M. Barazangi, Tomography of the western United States from regional arrival times, *J. Geophys. Res., 96*, 16,369-16,381, 1991.

Humphreys, E. D., and R. W. Clayton, Tomographic image of southern California mantle, *J. Geophys. Res., 95*, 19,725-19,746, 1990.

Humphreys, E. D., and K. G. Dueker, Physical state of the western U.S. upper mantle, *J. Geophys. Res.*, in press, 1993.

Humphreys, E. D., and B. H. Hager, A kinematic model for the Late Cenozoic development of southern California crust and upper mantle, *J. Geophys. Res., 95*, 19,747-19,762, 1990.

Iyer, H. M., and T. Hitchcock, Upper-mantle velocity structure in the continental U.S. and Canada, in Geophysical Framework of the Continental United States, edited by L. C. Pakiser and W. D. Mooney, *Mem. Geol. Soc. Am., 172*, 681-710, 1989.

Iyer, H. M, and A. Rite, Teleseismic *P*-wave delays in the Oregon Cascades, *Eos, Trans. AGU, 62*, 1089, 1981.

Iyer, H. M., J. N. Hitchcock, J. N. Roloff, and J. M. Coakley, *P*-wave residual measurements over the Battle Mountain heat flow high, Nevada, *Eos Trans. AGU, 58*, 1238, 1977.

Iyer, H. M., J. R. Evans, G. Zandt, R. M. Stewart, J. Coakley, and J. Roloff, A deep magma body under the Yellowstone caldera: Delineation using teleseismic *P*-wave residuals and tectonic interpretation, *Geol. Soc. Am. Bull., 93*, 1471-1646, 1981.

Jones, C. H., H. Kanamori, and S. W. Roecker, Missing roots and mantle "drips": Regional P_n and teleseismic arrival times in the southern Sierra Nevada and vicinity, California, *J. Geophys. Res.*, in press 1993.

Koizumi, C. J., A. Ryall, and K. F. Priestley, Evidence for a high-velocity lithospheric plate under northern Nevada, *Bull. Seismol. Soc. Am., 63*, 2135-2144, 1973.

LeFevre, L. V., and D. V. Helmberger, Upper mantle *P* velocity structure of the Canadian Shield, *J. Geophys. Res., 94*, 17,749-17,765, 1989.

Masse R. P., M. Landisman, and J.B. Jenkins, An investigation of the upper mantle compressional velocity distribution beneath the Basin and Range province, *Geophys. J. R. Astron. Soc., 30*, 19-36, 1972.

Meyerholtz, K. A., G. L. Pavlis, and S. A. Szpakowski, Convolutional quelling in seismic tomography, *Geophysics, 54*, 570-580, 1989.

Michaelson, C. A., and C. S. Weaver, Upper mantle structure from teleseismic *P* wave arrivals in Washington and northern Oregon, *J. Geophys. Res., 91*, 2077-2094, 1986.

Monfort, M. E., and J. R. Evans, Three-dimensional modeling of the Nevada test site and vicinity from teleseismic *P*-wave residuals, *U.S. Geol. Surv. Openfile Rep. 82-409*, 1982.

Montagner, J.-P., and T. Tanimoto, Global upper mantle tomography of seismic velocities and anisotropies, *J. Geophys. Res., 96*, 20,337-20,351, 1991.

Mooney, W. D., and L. W. Braile, The seismic structure of the continental crust and upper mantle of North America, in The Geology of North America, vol. A, *The Geology of North America-An Overview*, edited by A. W. Bally and A. R. Palmer, pp. 39-52, Geological Society of America, Boulder, Colo., 1989.

Mooney, W. D., and C. S. Weaver, Regional crustal structure and tectonics of the Pacific Coastal States: California, Oregon and Washington, in Geophysical Framework of the Continental United States, edited by L. C. Pakiser and W. D. Mooney, pp. 129-161, *Mem. Geol. Soc. Am. 172*, 1989.

Nolet, G., Solving or resolving inadequate and noisy tomographic systems, *J. Comput. Phys., 61*, 463-482, 1985.

Oppenheimer, D. H., and J. P. Eaton, Moho orientation beneath Central California from regional earthquake travel times, *J. Geophys. Res., 89*, 10,267-10,282, 1984.

Paige, C. C., and M. A. Saunders, LSQR: An algorithm for sparse linear equations and sparse least squares, *ACM Trans. Math. Software, 8*, 43-71, 1982a.

Paige, C. C., and M. A. Saunders, LSQR: Algorithm 582, LSQR: Sparse linear equations and sparse least squares, *ACM Trans. Math. software, 8*, 195-209, 1982b.

Parker, E. C., P. M. Davis, J. R. Evans, H. M. Iyer, and K. H. Olsen, Upwarp of anomalous asthenosphere beneath the Rio Grande Rift, *Nature, 312*, 354-356, 1984.

Priestley, K. F., and J. N. Brune, Surface waves and the structure of the Great Basin of Nevada and western Utah *J. Geophys. Res., 83*, 2265-2272, 1978.

Priestley, K. F., and J. N. Brune, Shear wave structure of the southern volcanic plateau of Oregon and Idaho and the northern Great Basin of Nevada from surface wave dispersion, *J. Geophys. Res., 87*, 2671-2675, 1982.

Raikes, S. A., Regional variations in upper mantle structure beneath southern California, *Geophys. J. R. Astron. Soc., 63*, 187-216, 1980.

Rasmussen, J., and E. D. Humphreys, Tomographic image of the Juan de Fuca plate beneath Washington and western Oregon using teleseismic *P*-wave travel times, *Geophys. Res. Lett., 15*, 1417-1420, 1988.

Romanowicz, B. A., Seismic structure of the upper mantle beneath the United States by three-dimensional inversion of body wave arrival times, *Geophys. J. R. Astron. Soc., 57*, 479-506, 1979.

Savage, M. K., P. G. Silver, and R. P. Meyer, Observations of teleseismic shear-wave splitting in the basin and range from portable and permanent stations, *Geophys. Res. Lett., 17*, 21-24, 1990.

Sheffels B., and M. McNutt, Role of subsurface loads and regional compensation in the isostatic balance of the Transverse Ranges, California: Evidence for intracontinental subduction, *J. Geophys. Res., 91*, 6419-6431, 1986.

Silver, P. G., and W. W. Chan, Implications for continental structure and evolution from seismic anisotropy, *Nature, 335*, 35-39, 1988.

Smith, R. B., M. M. Schilly, L. W. Braile, J. Ansorge, J. L. Lehman, M. R. Baker, C. Prodehl, J. H. Healy, S. Mueller, and R. V. Greensfeler, The 1978 Yellowstone-eastern Snake River Plain seismic profiling experiment: Crustal structure of the Yellowstone region and experiment design, *J. Geophys. Res., 87*, 2593-2596, 1983.

Spence W., *P*-wave residual differences and inferences on an upper mantle source for the Silent Canyon Volcanic Centre, southern Great Basin, Nevada, *Geophys. J. R. Astron. Soc., 38*, 505-523, 1974.

Spence, W., and R. S. Gross, A tomographic glimpse of the upper mantle source of magmas of the Jemez lineament, New Mexico, *J. Geophys. Res., 95*, 10,829-10,849, 1990.

Stewart, J. H., Tectonics of the Walker Lane belt, western Great Basin: Mesozoic and Cenozoic deformation in a zone of shear, in *Metamorphism and Crustal Evolution of the Western United States*, Rubey vol. VII, edited by W. G. Ernst, pp. 683-713, Prentice-Hall, Enlewood Cliffs, N. J., 1988.

Tarantola, A., and B. Vallete, Inverse problems = quest for information, *J. Geophys., 50*, 159-170, 1982.

Taylor, S. R., and H. J. Patton, Shear-velocity structure from regionalized surface-wave dispersion in the Basin and Range, *Geophys. Res. Lett., 13*, 30-33, 1986.

Thompson, G. A., R. Catchings, E. Goodwin, S. Holbrook, C Jarchow, C. Mann, J. McCarthy, and D. Okaya, Geophysics of the western Basin and Range province, in Geophysical framework of the continental United States, edited by L. C. Pakiser and W. D. Mooney, *Mem. Geol. Soc. Am. 172*, 177-203, 1989.

Walck, M. C., The *P*-wave upper mantle structure beneath an active spreading center: The Gulf of California, *Geophys. J. R. Astron. Soc., 76*, 697-723, 1984.

York, J. E., and D. V. Helmberger, Low-velocity zone variations in the southwestern United States, *J. Geophys. Res., 78*, 1883-1886, 1973.

Zandt, G., Seismic images of the deep structure of the San Andreas fault system, central Coast Ranges, California, *J. Geophys. Res., 86*, 5039-5052, 1981.

Zervas, C. E., and R. S. Crosson, P_n observation and interpretation in Washington, *Bull. Seismmol. Soc. Am., 76*, 521-546, 1986.

K. G. Dueker and E. D. Humphreys, Department of Geological Sciences, University of Oregon, Eugene, OR 97403.

(Received October 5, 1992; revised June 16, 1993; accepted June 22, 1993.)